NTNU
Norwegian University of
Science and Technology

Nanoparticles for Wound Closure

Christian Nordgaard Sundby

Master of Science in Physics and Mathematics
Submission date: June 2018
Supervisor: Rita de Sousa Dias, IFY

Norwegian University of Science and Technology
Department of Physics

Preface

This Master's Thesis is an expansion of my specialization project and a part of my degree in Biophysics and Medical Technology at the Department of Physics at NTNU.

First of all, I want to thank my fiancée Caroline Enevoldsen for bearing with me these last years of our student-lives. She is my light in the darkness, and I would not be where I am now without her. Literally, as she gets me up in the mornings.

I want to thank Rita de Sousa Dias for taking me on as her master student. I am grateful for having such an awesome supervisor, and it has been exciting working with her and the rest of the Rita Dias Group over this last year.

My thanks also go out to Gjertrud Maurstad, at the Department of Physics, for training in the lab and preparing stock solutions, and to Astrid Bjørkøy, also at the Department of Physics, for training and follow-up regarding the Leica SP5 microscope.

Gløshaugen, June 2018

Abstract

Studies have shown the potential of the application of nanoparticles in wound closure. In some cases, the nanoparticles have shown to aggregate in the wound, delaying the natural healing processes, which involve cell migration, diffusion of growth factors, *et cetera*. In this work we study the effect of the presence of nanoparticles on the diffusion of biomolecules of two different sizes.

Method optimization was a large part of the work to assess the permeability of the interface covered with TM-50 silica particles, using PDMA hydrogel as medium. Gel electrophoresis was used to evaluate the migration of salmon sperm DNA (1,320 kg/mol) across the nanoparticle interface, while confocal laser scanning microscopy was used to observe the permeability of the nanoparticle interface to fluorescent Dextran molecules (4.4 kg/mol).

From the electrophoresis setup it was found that the presence of nanoparticles do hinder the transport of relatively large DNA molecules across an interface. When using confocal laser scanning microscopy it was found that the best setup was a gel-gel interface, whereas the gels were pre-swollen. This setup was also a better model for wound closure *in vivo*. It was found that nanoparticles do not significantly affect the diffusion of relatively small polysaccharides across an interface.

Sammendrag

Nanopartikler har ifølge nyere forskning et potensiale innen lukking av sår. Sårheling innebærer prosesser som cellevandring og diffusjon av vekstfaktorer, og hvis nanopartikler aggregerer i et sår kan de dermed hindre det i å gro. Gjennom dette arbeidet har vi studert effekten nanopartikler har på diffusjon av molekyler av to ulike størrelser.

Det er lagt ned mye arbeid i utviklingen av gode metoder for å undersøke permeabiliteten til et grensesnitt dekket med TM-50 silisiumdioksidpartikler, med PDMA hydrogel som medium. Gel elektroforese ble benyttet til å vurdere vandringen til laksesperm DNA (1320 kg/mol) gjennom nanopartikkelgrensesnittet, mens konfokalmikroskopi ble brukt til å evaluere permeabiliteten til nanopartikkelgrensesnittet for Dextranmolekyler (4,4 kg/mol).

Nanopartiklene viste seg å hindre vandringen til de relativt store DNA molekylene i elektroforeseoppsettet. Konfokalmikroskopi viste seg å gi best resulteter når prøven besto av to geler limt sammen med nanopartikler, hvorav gelene var blitt svellet på forhånd. Dette oppsettet var også en bedre model for lukking av sår *in vivo*. Her påvirket for øvrig nanopartikkelgrensesnittet diffusjonen av de relativt små polysakkaridene til liten grad.

Contents

1 Introduction 1

2 Theory 3
- 2.1 Nanoparticle - hydrogel adhesion . . . 3
  - 2.1.1 Nanoparticles . . . 3
  - 2.1.2 Hydrogels . . . 3
  - 2.1.3 Nanoparticle - hydrogel interactions . . . 7
- 2.2 Interface permeability . . . 8
  - 2.2.1 DNA electrophoresis . . . 9
  - 2.2.2 Fluorescent molecule diffusion . . . 10

3 Materials and methods 15
- 3.1 Nanoparticle - hydrogel adhesion . . . 15
- 3.2 Interface permeability . . . 16
  - 3.2.1 Gel electrophoresis . . . 17
  - 3.2.2 Fluorescent molecule diffusion . . . 18

4 Results 21
- 4.1 Nanoparticle - hydrogel adhesion . . . 21
- 4.2 Interface permeability . . . 21
  - 4.2.1 Gel electrophoresis . . . 21
  - 4.2.2 Fluorescent molecule diffusion . . . 21

5 Discussion 33
- 5.1 Nanoparticle - hydrogel adhesion . . . 33
- 5.2 Interface permeability . . . 33
  - 5.2.1 Gel electrophoresis . . . 33
  - 5.2.2 Fluorescent molecule diffusion . . . 34

6 Conclusion 37

Bibliography 39

1 Introduction

Wound healing is a complex process, and with the skin protecting the body from the outside world, any rupture must be quickly and properly closed. The first wound treatments were described and recorded five millenia ago [1]. Several types of wound dressings have been developed and applied throughout the history of mankind, and in the 18th century surgery became a respected branch within the medicine-profession. Today there are thousands of wound care products available. In addition to a variety of sutures, staples, tissue glue, and adhesive tape, there is bioengineered tissue, negative pressure therapy, application of growth factors to stimulate wound healing, and the list goes on. Each method of wound closure has its pros and cons, and their suitability depend on the individual case and procedure. Many studies have been performed comparing wound closing techniques, in order to continually improve wound care [2–4]. Dumville *et al.* should be especially mentioned, as they have written a review on tissue adhesives for surgery, which is updated every 4 years or so [5]. For more details see reference [6].

In 2014, Meddahi-Pellé *et al.* performed a quite intriguing chain of experiments where they closed skin wounds in rats quite successfully with silica nanoparticles made by the Stöber method [7, 8]. The previous year, Rose, with a team partially overlapping with Meddahi-Pellé's team, glued hydrogels, as well as two pieces of calf liver with silica nanoparticles. It falls natural to compare the method of wound closure with nanoparticles to existing wound closuring techniques, especially tissue adhesives. Commonly used are octyl-2-cyanoacrylate (Dermabond), which is the only cyanoacrylate-based compound allowed as tissue glue [9]. Other glues, like fibrin-based tissue glue, exist, but do not provide sufficient tensile strength for closing skin wounds.

While Rose *et al.* tested the tensile strength of hydrogels glued with silica particles, Meddahi-Pellé *et al.* closed wounds and monitored the healing process. Their method of wound closure using nanoparticles was applied to both skin incisions as well as other tissues in wet conditions, like liver [7]. The nanoparticles were used both as an aqueous suspension and as a powder, yielding different results.

The end goal is to create, with silica nanoparticles, an alternative wound closing technique, with improved qualities from existing methods, and the potential for treatment of not only skin lacerations, but other tissues as well, like liver, spleen and kidneys [7].

Inspired by Rose and Meddahi-Pellé, experiments have been performed, approaching some of the challenges standing between the laboratory, and the surgery room. The focus in this project has been on determining the permeability through a glued interface in hydrogels, picking up where we left off in the specialization-project with DNA electrophoresis, and expanding with fluorescent biomolecule diffusion. Like in the specialization-work, nanoparticle-hydrogel adhesion experiments, as well as *ex vivo* nanoparticle-soft tissue adhesion experiments have also been carried out. The *ex vivo* experiments were carried out in collaboration with Corinna Dannert of the Rita Dias Group, and will not be discussed in this thesis.

2 Theory

2.1 Nanoparticle - hydrogel adhesion

One key aspect in this project has been finding a compatible system of nanoparticles and hydrogels, as the interface permeability experiments are based on the successful adsorption of polymers onto nanoparticles.

2.1.1 Nanoparticles

A particle with at least one of its characteristic dimensions within the range of $1-100$ nm is defined as a nanoparticle [10]. Nanoparticles have huge specific surface areas, and may exert quantum effects. They tend to agglomerate, resulting in clusters that may be difficult to disperse. Nanoparticles can occur naturally, or they can be man-made. Many of their properties are related to their size and eventual porosity. They were originally designed as molecular sieves, but are now applied in medicine, biosensors, thermal energy storage, and imaging [11, 12]. Mesoporous nanoparticles have been used with good results for *in vivo* targeted drug delivery especially for cancer therapy in small animals [12]. A mesoporous material is a material with small pores/holes of uniform size, with the pore-size ranging between $2-50$ nm [10]. This confers these particles a large surface area, ideal for adsorption and release of drugs. Another variant is amorphous nanoparticles, which have an arbitrary, or ill-defined internal structure [13]. Colloidal silica, schematically shown in Figure 1, are dense amorphous particles composed of SiO_2, which have been used in a number of applications like microelectronics and chromatography [14]. Silica nanoparticles possess charge in certain pH ranges, with their charge density increasing with pH, and decreasing with particle size [11]. In this work we have used amorphous silica [7, 15].

2.1.2 Hydrogels

Hydrogels are crosslinked polymers that form a three-dimensional network that can absorb water and swell [16]. The polymers are synthesized by free radical reactions that join monomers together through the formation of covalent bonds to form macromolecules [17]. As Ahmed explains in her quite thorough review on hydrogels in 2015, they can be classified on several bases, one of which being the type of crosslinking [13]. Chemical crosslink junctions are permanent, while physical junctions arise from either entanglement of polymer chains or from physical interactions such as ionic interactions, hydrogen bonds, or hydrophobic interactions, and are transient.

Having a defined geometry and not flowing like a liquid, hydrogels behave like solids, macroscopically that is, assuming the experimental time is shorter than the lifetime of the crosslinks [16]. On the other hand, a hydrogel can act as a solution, in which soluble molecules can diffuse depending on the network mesh size. A lot of attention has been given to hydrogels in the past 50 years, because of their potential in a wide range of applications [13]. Due to their high water content they show

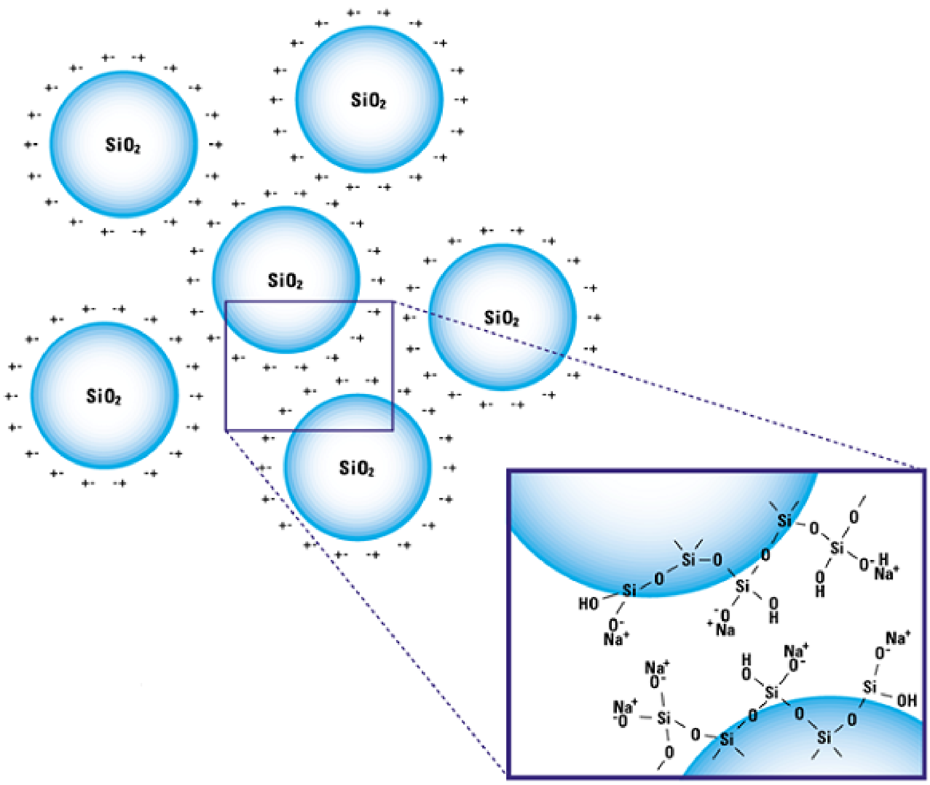

Figure 1: Colloidal silica (Source: Merck Performance Materials, 2017 [15]).

a large flexibility, much like natural tissue. Synthetic gels provide higher swelling ability, stronger gels, and longer lifetime than natural gels, and have replaced natural gels for the last decades [13]. Most synthetic polymers possess a well-defined structure allowing production of gels with fine-tuned functionality and degradability. Synthetic hydrogels are also quite resistant to changes in temperature. The mass fraction of water in a hydrogel is typically a lot larger than the mass fraction of polymer, and to achieve a high degree of swelling, synthetic polymers that are water-soluble when not crosslinked are commonly used. Polymer networks can be synthesized with control of parameters like density of the crosslinks, biodegradation, mechanical strength, and chemical and biological response to stimuli. Gels can also be tuned to swell or collapse under various conditions like temperature, ionic strength, pH, light, electric or magnetic fields, and so on. The mechanical behaviour of hydrogels in relation to their applications is an active field of research [16, 18].

Hydrogel swelling

A polymer network cannot be completely dispersed in a solvent, usually water, due to its crosslinks, but it can swell, or absorb water, however. The hydrophilic functional groups on the polymeric backbone are what gives hydrogels an affinity for water, and the entropy of mixing of the polymers and water is what drives the system toward swelling. The systems elasticity, or resistance toward swelling, derives from the crosslinking of the network chains. Charged polymer networks swell more due to the osmotic pressure of the counterions inside the network. The swelling equilibrium is reached when the osmotic pressure inside the gel, Π_{gel}, is equal to that of the solvent, Π_{out}, described by the following relation:

$$\Pi_{\text{gel}} = \Pi_{\text{mix}} + \Pi_{\text{elas}} + \Pi_{\text{ion}} = \Pi_{\text{out}} \,, \tag{1}$$

where Π_{mix}, Π_{elas} and Π_{ion} are, respectively, the mixing, elastic, and ionic contributions to the osmotic pressure [16, 17, 19].

PDMA

Poly(dimethylacrylamide) gels are self-crosslinked hydrogels, prepared only from water, monomer and initiator [16]. The hydrogels are made by free-radical polymerization of dimethylacrylamide in aqueous solution, with potassium persulfate (KPS) and tetramethylethylenediamine as redox initiators. Figure 2 shows the different reactions taking place during polymerization, induced by KPS, and how self-crosslinking can occur [18]. Methylenebisacrylamide can also be added in very small amounts as a chemical crosslinking agent. It increases the quantity of crosslinks, thereby altering the mechanical properties of the gel [20].

Rose, Carlsson, Sudre and respective co-authors described the effect the presence of oxygen during the polymerization process would have on the surface properties of PDMA [16, 21, 22]. The gels should be cast in a nitrogen environment and the surface of the mold should be hydrophobized. This is because oxygen may adsorb to the mold surface causing a slightly lower polymerization in the surface than in the deeper layers of the gel, resulting in changes to the friction and adhesion properties of the gel.

Agarose

Agarose gel consists of helical agarose molecules in supercoiled bundles that are aggregated into a three dimensional matrix through which biomolecules can pass. The gel structure is held together by hydrogen bonds, and the gel can therefore be heated back to liquid state. Agarose has large pore size and good gel strength, making it a suitable anticonvection medium for electrophoresis of DNA and large protein-molecules. The average pore size of a 1 % agarose gel is estimated to be $100 - 500$ nm [23–25].

Alginate

Alginate, in the form of hydrogel beads, is widely used as a medium for encapsulation within biomedicine, bioprocessing, and pharmaceutical applications. It is a natural hydrogel as it is a polysaccharide derived from brown seaweed, which is edible, and has been consumed in Asia since ancient times. These marine algae are a rich source of fiber, minerals and protein, and the polysaccharide is found in their cell walls. The structure of alginate is composed of linear binary copolymers

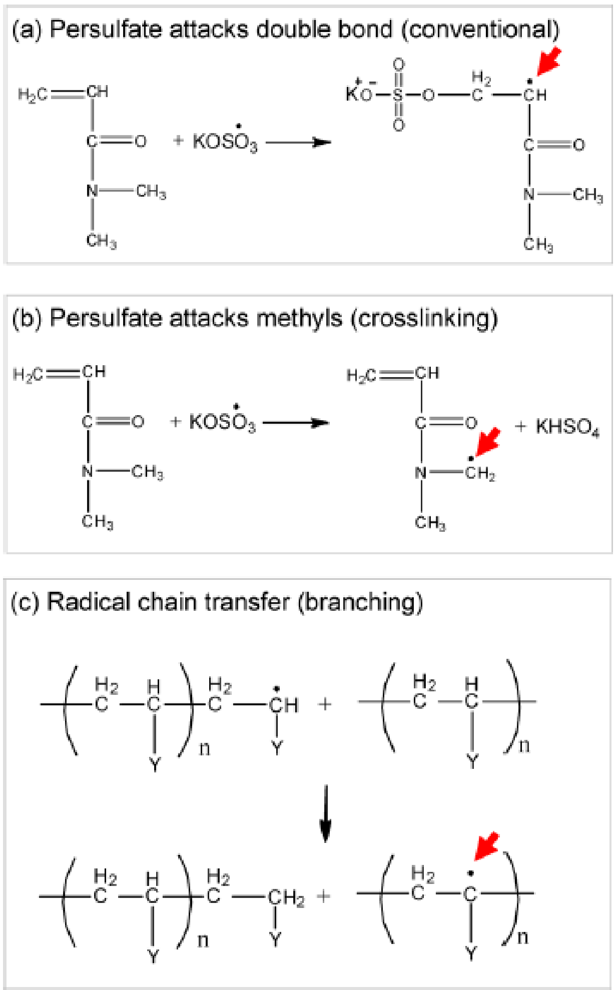
(a) Persulfate attacks double bond (conventional)
H2C=CH
C=O
N—CH3
CH3
+ KOSO3
KO—S—O—C—CH
(b) Persulfate attacks methyls (crosslinking)
+ KHSO4
CH2
(c) Radical chain transfer (branching)
H2
H
C
CH
Y
n
CH2

Figure 2: The possible reactions during polymerization of dimethylacrylamide initiated by KPS (Source: Cipriano *et al.*, 2014 [18]). **a** Persulfate radicals facilitate the formation of linear polymer chains. **b** A hydrogen is removed from a methyl group, allowing it to connect to another chain thus forming a crosslink. **c** Chain transfer, forming branches and junctions between linear chain segments. Red arrows marks the radical on the growing polymer chain.

of 1 → 4 linked α-D-mannuronic acid (M block) and β-L-guluronic acid (G block) [26–28]. For many applications it is desirable that the alginate beads are monodisperse in size and spherical in shape, and it is therefore critical to be able to control these properties. Alginate beads are often prepared using extrusion dripping, where several factors influence the size and shape of the beads, such as solution viscosity, nozzle size, and collecting distance [26, 29].

2.1.3 Nanoparticle - hydrogel interactions

The mechanisms of nanoparticle - hydrogel interactions are not yet fully understood, but strong, fast adhesion between two hydrogels can be achieved with silica nanoparticle solution, as shown by Rose *et al.* in 2013 [21]. In order to work and function as a glue, the surface of the nanoparticles must have an affinity towards the network chains. That is, the free energy gain, ϵ, from the adsorption of a monomer to the surface of a particle should be at least comparable with the thermal energy kT. It is expected that many monomers per network strand are adsorbed onto one particular particle, and for nanoparticles with diameters comparable to the network mesh size, several different strands are adsorbed to the same particle. The nanoparticles thus act as connectors between two pieces of gel, and the network-chains act as bridges between the particles as illustrated in Figure 3. If the adhesive junction is strained, tension is placed on the adsorbed chains, resulting in some monomers detaching from the surface of the particle which relieves the tension. The energy dissipated from this desorption is much higher than ϵ, which is what results in the good adhesive quality. While chain breaking, in order to dissipate energy under stress, would have been irreversible, here, the desorbed monomers can always adsorb again and in fact monomers are continuously adsorbing and desorbing. Also, neighbouring strands may adsorb and replace a detached link. These exchange processes and the dissipation of energy yield strong adhesion, and make the junction resistant to interfacial fracture propagation [21, 30].

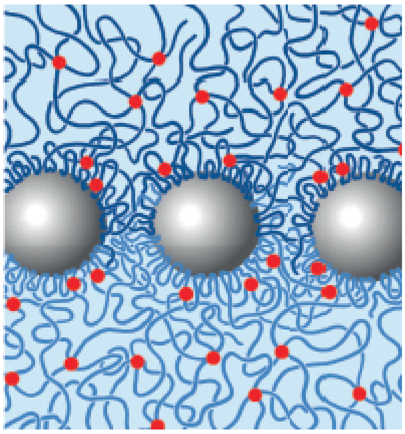

Figure 3: Illustration showing how a layer of nanoparticles connects two hydrogels, and the polymer chain in the gels acting as nanobridges between the nanoparticles (Source: Rose *et al.*, 2013 [21]).

Another aspect of nanoparticle adhesion is their ability to remain adsorbed at the interface. A study was conducted in 2016 by Cao *et al.*, where they used molecular dynamics simulations and theoretical calculations to establish conditions for different regimes of interfacial confinement of nanoparticles between two polymeric gels [31]. Nanoparticles in contact with two elastic surfaces can adapt either a bridging state, a pickering state or a submerged state, as illustrated in Figure 4. The particular configuration is the result of a balance between the elastic energy of the

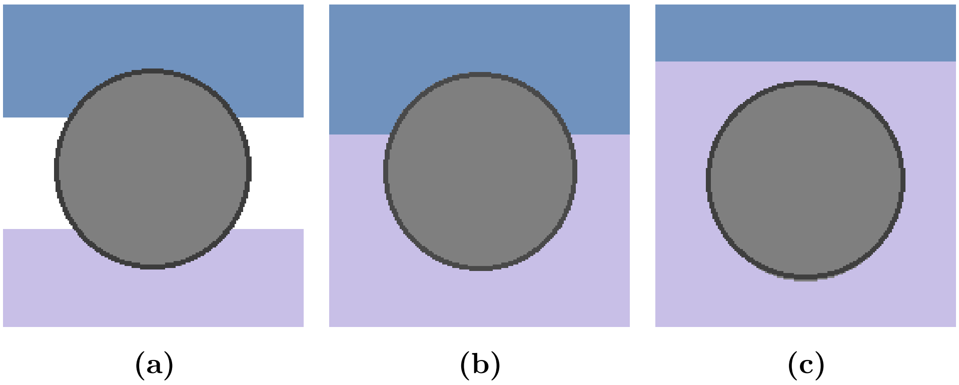
(a) (b) (c)

Figure 4: Illustration showing the interaction of nanoparticles with two gel surfaces [31]. **a** Bridging state, more favorable for hard gels and large nanoparticles. **b** Pickering state, more favourable for soft gels and smaller nanoparticles. **c** Submerged state, where nanoparticles are smaller than the pore size of the gel. No bridging is achieved in the latter state.

indentations in the gels made by the nanoparticles, and the free energy change due to changes in contact area of the nanoparticles and the gels. For large nanoparticles interacting with hard gels, the bridging state is more favorable, while the pickering state is more favorable for small nanoparticles interacting with soft gels [31].

Also worth mentioning is the work of Tang *et al.* who in 2016 used nanoparticles to improve the adhesion between a hydrogel and an elastomer [32]. The interactions between nanoparticles and polymer chains may include hydrogen bonding and ionic adsorption. In their work, silica nanoparticles was used for gluing hydrogels. The surface of amorphous silica is complex and consists of different functional groups, one of them being silanol (Si-OH). The negative charge on the particle surface comes from the dissociation of the hydroxyl ions (OH^-), which again reacts with protons in the solution to form water. This surface charge will make the particles repel one another and disperse, rather than agglomerate. Tang measured the zeta potential of Ludox TM-50 (Aldrich) to −35 mV at pH 9, and confirmed the previous knowledge that silica is negatively charged. The weak adhesion between a hydrogel and an elastomer without nanoparticles are due to weak van der Waals interactions and the repulsive steric interactions between polymer chains. The addition of nanoparticles increase the adhesion between acrylic elastomer and gels like PAAm, PDMA and PNIPAM, but not for PAA. The reason for this is that the polymer backbone of PAA hydrogels carries a great density of negative charges at high pH. This creates electrostatic repulsion between PAA monomers and silica nanoparticles, which lowers the adhesion. The polymer backbone of the other gels are neutral however, and do not interact electrostatically with the silica nanoparticles [32].

2.2 Interface permeability

Gluing skin wounds with nanoparticles should hopefully provide an interface that is permeable to biomolecules. During recovery from skin lacerations there is cell migration, diffusion of growth factors, and other processes that are crucial for proper healing. If these processes are hindered, the healing process might be severely set back [33]. Meddahi-Pellé *et al.* closed a wound in rat skin using nanoparticles both as an aqueous solution and as a powder. The difference in the outcome proved quite substantial; the rat skin wounds glued with silica suspension turned out to heal fast and properly, while in the case of the powder silica application, the granulation tissue did not develop. One explanation for this may be the formation of a rigid macroscopic barrier caused by the aggregation of the nanoparticles in the dry form. In this work we explore the permeability of the nanoparticle interface to molecules of two different sizes, DNA with 1,320 kg/mol, and fluorescent Dextran with 4.4 kg/mol. Gel electrophoresis was used to study the permeability of a nanoparticle interface to long DNA molecules, while confocal laser scanning microscopy was used to study the permeability of a nanoparticle interface to short Dextran molecules (polysaccharides).

2.2.1 DNA electrophoresis

Gel electrophoresis is a standard procedure for separating DNA by size, that is, in length in base pairs. A voltage is applied, and one exploits the negative charge of the phosphate backbone of DNA when it travels through the gel matrix toward the positive electrode, described by the following equation:

$$v = \frac{Eq}{f}\,, \tag{2}$$

where v is the velocity of the molecule with charge q, E is the electric field in V/cm, and f is the friction coefficient. Shorter DNA fragments travel faster than long ones, and one can determine the length of the DNA fragments by running alongside DNA fragments of known length, called a DNA ladder. Since the length the DNA travels depends on its size and the pore dimensions of the gel, it is essential to find the right conditions to run the desired DNA molecules. High concentration gels lead to longer run time, and for standard agarose electrophoresis larger molecules are resolved better with lower concentration gels, while smaller molecules separate better with gels with higher concentrations. The rate of migration is proportional to the voltage applied, but high voltages will decrease the resolution of large DNA fragments. The ionic strength of the buffer may also affect the migration of nucleic acids [25, 34].

A hydrogel suitable for electrophoresis must be stable throughout the run. Additionally, it should withstand the voltage and heat that follows electrophoresis [25].

DNA digestion

The size of the DNA fragments in a DNA sample can be reduced by digesting it with DNase. DNase is a nuclease, that is, an enzyme that degrades nucleic acids. Some nucleases are DNA specific (DNase), some are RNA specific (RNase) and some degrade both. Deoxyribonuclease, or DNase, catalyzes the hydrolytic cleavage of

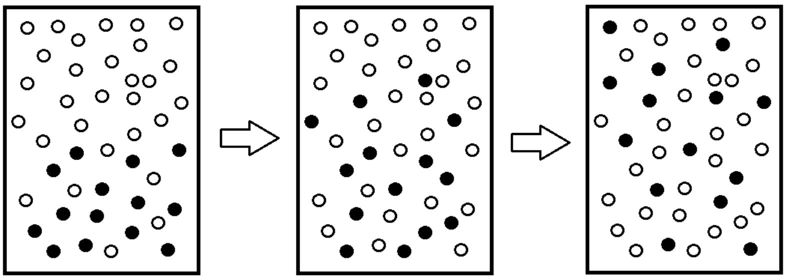

Figure 5: Diffusion from an initially sharp boundary between solvent (top) and solution (bottom). The system initially possess a maximum of free energy and a minimum of entropy, and as the system reaches equilibrium the free energy is at a minimum, while the entropy is at a maximum [38].

phosphodiester linkages in the backbone of DNA, thus degrading the DNA. The DNases are classified according to whether they cut, or cleave, from the end of a DNA molecule (an exodeoxyribonuclease, a type of exonuclease) or from anywhere along the chain (an endodeoxyribonuclease, a type of endonuclease) [35].

Staining

A loading dye is added to the sample, in order to monitor the migration through the gel during electrophoresis. However, this dye travels independently of the DNA, and can only be used as a reference to estimate when to end the run. For actual visualization of the DNA, a DNA-specific fluorescent dye is added by pre-staining or post-staining. When the electrophoresis run is done, the gel is placed in a transilluminator and the DNA bands appear [34].

In this work GelStar was used as the fluorescent dye. GelStar is a nucleic acid gel stain, with excitation maxima at 493 nm, and emission maxima 527 nm (532 nm) for DNA (RNA). It has an additional excitation peak around 300 nm which allows for use with standard UV transillumination systems [36].

2.2.2 Fluorescent molecule diffusion

Diffusion

There are two ways to explain the basics of diffusion: Either a phenomenological approach with Fick's laws and their mathematical solutions, or a physical and atomistic one, where one considers the random walk of the diffusing particles. Based on the latter, diffusion is defined as the net movement of molecules or atoms from high to low concentration as a result of random motion. The diffusion is driven by a gradient in chemical potential of the diffusing species. A gradient is the change in either concentration, temperature or pressure over some distance. The result of diffusion is mixing, or mass transport without requiring directed bulk motion. The spreading of an initially sharp boundary by diffusion is illustrated in Figure 5 and 6 [37, 38].

Random walk is a stochastic process that describes a path created by random

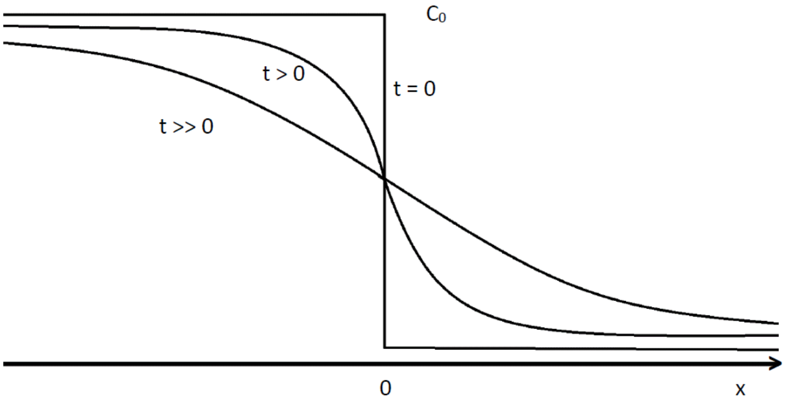

Figure 6: Spreading of an initially sharp boundary by diffusion [38].

steps. Brownian motion is a time-dependent diffusion model based on random walk of particles suspended in a fluid, being it a liquid or a gas, resulting from their collisions with the fast moving molecules in the fluid [37].

The jump model is a diffusion model based the jumps of molecules to the nearest free space. One consider a lattice where each diffusing molecule occupies a space, and some of the places are free. A molecule in this lattice can move to a vacant space, or trade places with a neighbouring molecule [39].

Confocal laser scanning microscopy

When imaging thick specimens, like tissue samples or rounded cells, with conventional widefield optical systems, fluorescent objects outside the focal plane increase the background signal, which results in low-contrast images. Confocal microscopy solves the problem by ignoring contributions from above or below the focal plane. That is accomplished by illuminating the sample with a focused laser scanning beam and having a pinhole aperture placed in the image plane in front of an electronic photon detector [40].

Optical principle

A confocal microscope is an integrated system consisting of a fluorescence microscope, laser light sources, a scan head, a computer with associated software for configuration, acquiring, processing and analyzing images, as illustrated in Figure 7. The scan head consists of several components: input from external laser light sources, fluorescence filter sets, a raster scanning mechanism, pinhole apertures for creating the confocal image, and photomultiplier tube (PMT) detectors. The optical principle of confocal laser scanning microscopy (CLSM) is illustrated in Figure 8 and is described as follows [40, 41]:

- Epi-illumination is applied, where the detector and the light source are placed on the same side of the specimen plane, and separated from it by the objective, which functions as both a condenser and an objective. The fluorescence filter

Figure 7: The setup for the Leica SP5 microscope (Source: Leica Microsystems, 2018 [42]).

sets (exciter filter, dichroic filter, and emission filter) works as in widefield fluorescence microscopy.

- In a procedure called point scanning, a laser beam fills the rear aperture of the objective creating a diffraction-limited spot that is scanned over the specimen in a raster pattern.

- The pinhole aperture receives fluorescent photons from the illuminated focused spot in the raster, excluding photons originating from above or below the focal plane. The pinhole also eliminates a lot of stray light in the optical system. This is illustrated in Figure 8. The combination of point scanning and the pinhole aperture as a spatial filter is essential for obtaining a confocal image.

- The photomultiplier tube produces a voltage corresponding to the intensity of the incident fluorescent photons. The computer digitizes the signal and displays it on a monitor.

- An image can be generated of an extended specimen in a process called descanning, where the laser beam is scanned across the object, in the x- and y-plane, in a raster pattern typically based on two high-speed vibrating mirrors that oscillate in mutually perpendicular directions (along the x- and y-axes). The speed of the mirrors is inconsequential relative to the speed of light, therefore, fluorescent light follows the same path on its return and is brought to the same position on the optical axis as the original exciting laser beam. The photons then pass through a dichromatic mirror and become focused at the confocal pinhole. The image in the pinhole remain steady at all times since descanning is instantaneous.

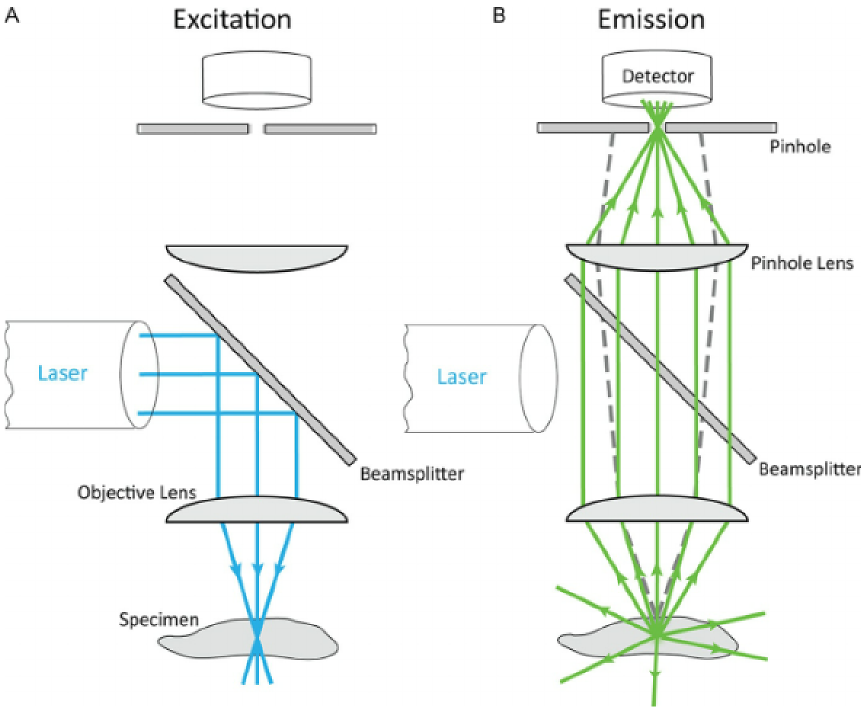

Figure 8: The confocal principle in laser scanning microscopy, with the excitation (**A**) and emission (**B**) light paths separated for clarity. The laser beam is focused to a scanning point in the specimen. Emission from that point in the specimen will have a confocal point at the detector pinhole after passing through the objective. The pinhole will largely exclude fluorescent light emitted from points above (dotted line) or below the focal plane. The emission filter is not shown (Source: Jonkman *et al.*, 2014 [43]).

- The PMT converts the fluctuations in light intensity into a continuously changing voltage. This analog signal is digitized at time intervals by an analog-to-digital converter to generate digital picture elements (pixels). These are displayed on a monitor and thus a confocal image of an object has been reconstructed from fluorescent photon signals.

Image quality

There are four principal factors determining image quality [40]: spatial resolution, resolution of light intensity (dynamic range), signal-to-noise ratio, and temporal resolution. Temporal resolution depends on the raster scan rate, the detector processing rates, the analog-to-digital converter, and the computer. A typical frame is captured at 1-2 Hz for a 512 × 512 pixel image, but for an image of limited size rates can be 100 Hz or higher [40, 44, 45].

3 Materials and methods

3.1 Nanoparticle - hydrogel adhesion

This section will present the materials and procedures for making the gels used. Adhesive properties of agarose and PDMA with nanoparticles were tested in the specialization project. In this semester adhesion work was expanded to alginate gels.

Materials

The only chemical used for making agarose gel was agarose (Sigma). The chemicals used for the PDMA gels were N,N-Dimethylacrylamide (DMA, 99%, Aldrich), potassium persulfate (KPS, 99.99%, Aldrich), N,N,N',N'-tetramethylethylenediamine (TEMED, ∼99% redistilled, Sigma Aldrich) and N,N'-methylenebisacrylamide (MBA, Sigma). Alginate (sample obtained from the Department of Biotechnology and Food Science) and calcium chloride dihydrate (ACS reagent $\geq$ 99%, Sigma Aldrich) were used to prepare alginate beads. The nanoparticles were Ludox silica TM-50 and SM-30 (Aldrich). They are listed in Table 1.

Table 1: The table lists the two amorphous nanoparticles used throughout the experiments, both being water solutions (Source: Sigma Aldrich, 2017 [46, 47]).

Nanoparticles	**Radius** nm	**pH**	**Surface area** m^2/g	**SiO_2/Na_2O** ratio	**Concentration** wt%
TM-50	15*	8.5 – 9.5	110 – 150	200 – 250	49 – 51
SM-30	5*	9.7 – 10.3	320 – 400	45 – 56	29 – 31

*The radii of the silica particles are taken from Rose *et al.* 2014 [21]. They performed scanning electron micrographs to identify the radii of the same silica nanoparticles.

Preparation of PDMA

The composition of the PDMA gels are listed in Table 2. They were prepared using the method described by Carlsson *et al.* [16]; the gels were prepared in a fumehood at room-temperature, by free-radical polymerization of DMA with KPS and TEMED as redox initiators. MBA was added as a chemical crosslinker. Since some of the chemicals are toxic, stock solutions were prepared by Gjertrud Maurstad as follows: DMA 0.1924 g/mL, KPS 0.0082 g/mL, MBA 0.1346 g/mL. TEMED was used as received. All the PDMA gels were made with a molecular ratio of DMA/KPS/TEMED set to 100/1/1. Only the MBA/DMA ratio was varied, and throughout the work PDMA was prepared with 0.05 mol% MBA and 0.1 mol% MBA. These will be referred to as soft and hard gels, respectively. Both gels are prepared in the same way, with their appropriate amounts of chemicals (Table 2). To prepare a 15 mL soft gel solution, 7.72 mL DMA stock solution was mixed with 0.0845 mL MBA stock solution and 2.24 mL ultrapure water. Then 4.94 mL of KPS stock solution was added, and the preliminary solution purged with nitrogen for 3 minutes, in order to remove oxygen. Finally, 22.5 μL of TEMED was added, and the solution was quickly poured into a mold and lidded. The PDMA solution was left overnight to polymerize.

Table 2: The table presents the composition of the PDMA gels used in these experiments. The soft gel has 0.05 mol% of MBA, while the hard gel has 0.1 mol%. The gels were prepared using the method of reference [16].

Sample	**DMA**/g	**MBA**/g	$\mathbf{H_2O}$/mL	**KPS**/g	**TEMED**/μL
Soft	1.485	0.0012	14.98	0.0405	22.5
Hard	1.485	0.0023	14.98	0.0405	22.5

Preparation of Agarose

Agarose was prepared as a 0.9 wt% solution, following the procedure described in reference [34]. 0.81 g of agarose was dissolved in 90 mL ultrapure water and heated under magnetic stirring until nearly boiling. The solution was then cooled down to 50°C before poured into the casting tray of the electrophoresis chamber. The comb was immediately placed onto the tray, and some minor airbubbles were pushed to the sides of the chamber with a spatula. The gel was left for at least 30 minutes to harden.

Preparation of alginate beads

Calcium alginate hydrogel beads were produced by extrusion dripping, as described by Lee *et al.* [26]. To make a 2 wt% alginate solution, 0.2 g of sodium alginate was dissolved in 10 mL MQ water under magnetic stirring. The solution was left for 30 minutes to release trapped air bubbles. A typical concentration of calcium chloride used for Ca-alginate bead formation is 0.1 M [26]. A solution of this concentration was prepared by dissolving 0.111 g $CaCl_2$ in 10 mL MQ water. The alginate solution was dripped into the calcium solution under magnetic stirring. In order to produce larger beads, a disposable Pasteur pipette with a clipped off tip was used to allow for a slightly larger dripping nozzle diameter. The final beads had diameters around 4-5 mm. Some much larger beads were also achieved by lowering a teaspoon with alginate solution gently into the calcium solution. Those beads were about 15 mm in diameter. Some alginate beads were also colored by adding a food colorant (Dr. Oetker) into the alginate solution.

3.2 Interface permeability

To investigate the permeability of the nanoparticle-covered gel interface we used two approaches. The diffusion of large DNA was investigated using gel electrophoresis, and the diffusion of smaller fluorescent Dextran molecules was followed using confocal laser scanning microscopy.

3.2.1 Gel electrophoresis

Materials and equipment

Two sources of DNA were used for the electrophoresis: Salmon sperm DNA (Invitrogen), and GeneRuler 1kb DNA Ladder (Thermo Fischer Scientific). DNase, DNase buffer, and Inactivation Reagent from the TURBO DNA-free Kit (Thermo Fischer Scientific) were used for DNA digestion. Gel Loading Dye Purple 6× (New England BioLabs) and GelStar Nucleic Acid Gel Stain (Lonza) were used for running- and UV-visualization, respectively. The running buffer for the electrophoresis was Tris-Borate-EDTA (TBE, Thermo Fischer Scientific), supplied as a 10× solution.

For incubation, a TW12 Water Bath (Julabo) was used. The electrophoresis setup consisted of a kuroGel Mini Plus 10 Horizontal chamber (VWR) with a 250 V power source (VWR). A 3UV Benchtop Transilluminator (UVP) was used for visualizing the bands.

DNA digestion and staining

The salmon sperm DNA, which is polydisperse in size, and with an average size of $\leq$ 2,000 bp, was received as a 10 mg/mL solution and diluted to 0.2 mg/mL with Tris HCl buffer. 25 μL of DNA solution was mixed with 2.5 μL of DNase buffer in an Eppendorf tube. Then 0.5 μL DNase was added, and the solution was incubated at 37°C for the desired amount of time. Then, 2.5 μL Inactivation Reagent was added, and the solution was incubated at 20°C for 5 minutes under occasional mixing.

For staining, 59.5 μL TBE buffer was mixed in an Eppendorf tube with 25 μL of the digested DNA solution. Then 0.5 μL GelStar was added, and the solution left for some time to equilibrate. Afterwards, 15 μL of loading dye was added to the sample. The final concentration of DNA was 47 μg/mL.

The DNA ladder contains 14 fragments ranging from 250 bp to 10,000 bp, and was received as a 0.5 mg/mL solution. For preparing a sample of DNA ladder, which already contained loading dye, 35 μL of TBE buffer was mixed with 5 μL DNA solution. Then 0.5 μL GelStar was added and also this solution left to equilibriate. The final concentration of ladder DNA was 62 μg/mL.

Running electrophoresis

The PDMA solutions were prepared as 60 mL solutions, and poured in the casting tray of the electrophoresis chamber. A custom-made lid was made for this project. It prevented the contact of gel with oxygen, to ensure proper polymerization, and it had an integrated comb to create the wells. The glass lid was not hydrophobized, as suggested by references [16, 21, 22], but simply cleaned with acetone. After hardening, the gel was cut about half way across and then glued back together with TM-50 before the electrophoresis chamber was filled up with TBE buffer to cover the gel entirely. The agarose gels were prepared by simply pouring the agarose solution directly into the casting tray. The original comb was inserted, and no lid was required. The DNA samples were loaded into the wells with a pipette, before

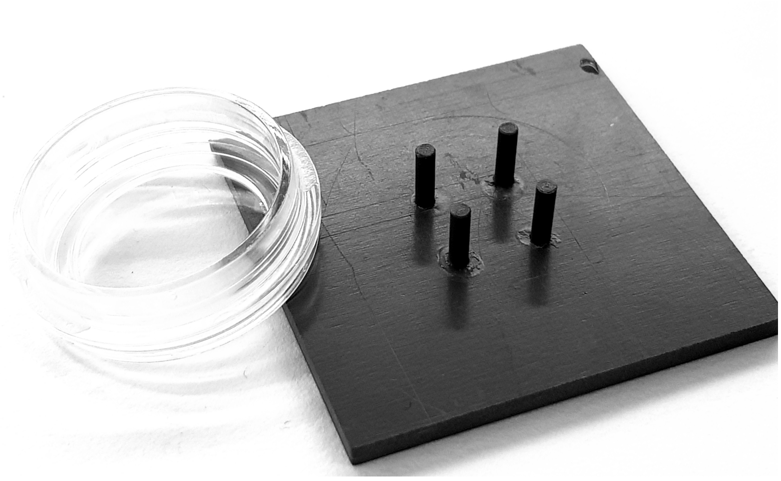

Figure 9: Image showing the chamber slide and custom-made lid for preparing gels for the fluorescent molecule diffusion experiment.

the voltage (constant at 40 V) was applied and electrophoresis initiated. The DNA bands were visualized at 302 nm since GelStar has a small emission peak around 300 nm [34, 36].

3.2.2 Fluorescent molecule diffusion

As an introduction to the experiments with the fluorescent molecule, and a proof-of-concept, food colorant was used to assess diffusion across a nanoparticle-coated PDMA gel surface. This was done by casting a hard gel in two small tubes, with pipette tips inserted to create wells. One of the wells was filled with nanoparticles (TM-50), and to the other well the same amount of water was added. After 2 minutes the excess water and solution was carefully removed, leaving one well bare, and a coat of nanoparticles in the other. Finally, food colorant diluted in water to a 1:1 (v/v) ratio was poured into the wells, and its diffusion into the gel observed. Based on the observation made, this introductory experiment was expanded to follow the diffusion of a fluorescent biomolecule through a nanoparticle barrier, using confocal laser scanning microscopy.

Materials and instrumentation

Tetramethylrhodamine isothiocyanate-Dextran (TRITC-Dextran, Mw = 4,400, from Sigma) was used as fluorescent dye. PDMA was used as a medium for diffusion. The nanoparticles used as coat/glue were TM-50 (Table 1). The instrumentation was a Leica TCS SP5 confocal laser scanning microscope, with the setup as illustrated in Figure 7. For measuring fluorescence of samples a SpectraMax i3x spectrophotometer (Molecular Devices) was used.

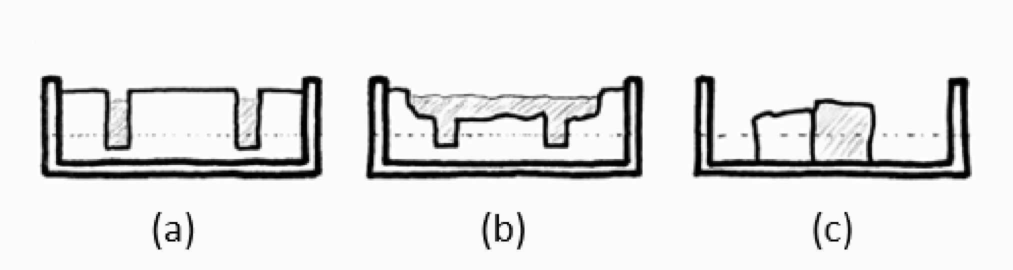

Figure 10: Illustration of the different experimental setups for the fluorescent molecule diffusion experiments. It shows the cross-section of the chamber slide in which the gel was polymerized, and the dotted line shows the plane in which the sample was imaged with CLSM. **a** Solution-gel setup, to image diffusion from the Dextran solution (grey) in the wells radially outwards into the gel (white). One well was coated with nanoparticles, while the other was coated with water. **b** Same setup, but with the top of the gel carved away to create a reservoir of Dextran solution. **c** Gel-gel setup, where one gel has been swollen in water (white), and the other has been swollen in Dextran solution (grey), to image diffusion from one gel to the other.

Procedure

Dextran was prepared as a stock solution of 0.195 mg/mL. PDMA was prepared as described previously, as both soft and hard gels (Table 2), to a total volume of 15 mL, and poured into round chamber slides. The chamber slides were lidded immediately to protect the polymerization process from oxygen as previously explained [16, 21, 22]. Also in these experiments the lids were custom-made, including rods to create wells in the gel (Figure 9 and 10a). The rods had a diameter of 2 mm. As in the introductory experiment, one well was coated with nanoparticles, and another was left bare. Dextran solution was then added to each well, and the diffusion of the fluorescent Dextran through the presumably coated or naked gel surfaces could be visualized in the confocal microscope. A few variations of the setup were tried out, as illustrated in Figure 10. One variant involved carving out a big portion of the gel to create a reservoir of dextran solution (Figure 10b), another involved pre-swelling the gels, and a third option was gluing two pieces of gel together, whereas one has been equilibrated in a Dextran solution, and the other in water (Figure 10c).

During the specialization work, conducted in the previous semester, it was discovered that GelStar would form a complex with the TM-50 nanoparticles, which could provide a good way to image the nanoparticles present at the gel-gel interface. Two pieces of gel were glued together with a solution of 40 μL TM-50 and 0.5 μL GelStar, and then imaged. The experiment was also carried out after swelling the gels in water overnight.

To see if the presence of nanoparticles would affect the emission from Dextran, the fluorescence emission of Dextran, and Dextran with nanoparticles, was obtained using the SpectraMax. The nanoparticle solution alone was also investigated as a control.

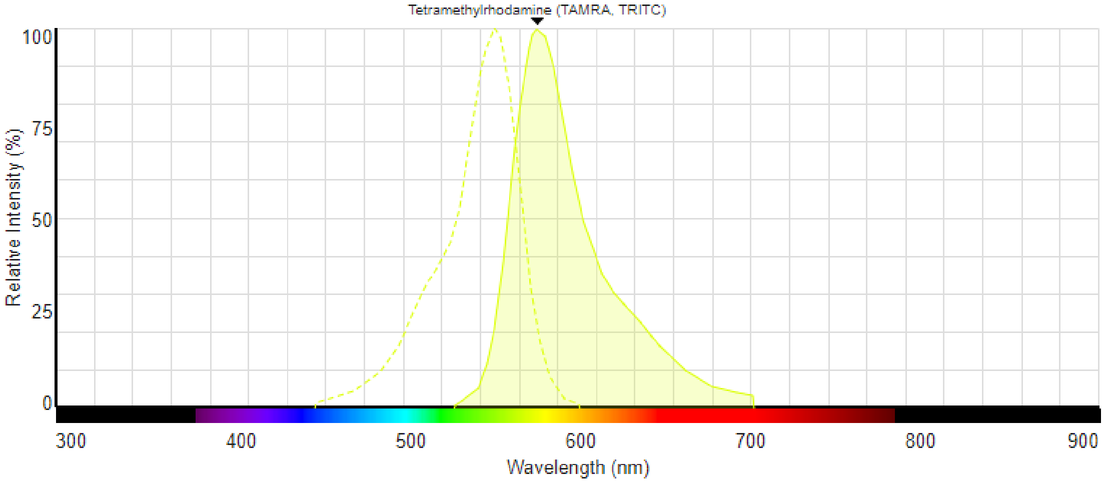

Figure 11: Spectra showing wavelengths of excitation (λ_{ex}) and emission (λ_{em}) for the fluorophore Dextran. The dashed line is excitation while the continuous line is emission (Source: Thermo Fischer Scientific, 2018 [49]).

Image acquisition and processing

In order to follow the process of diffusion, 5 images were taken with 10 minutes apart. The images were captured at a rate of 100 Hz, with a pixel size of 512 × 512. The frame size was 3.10 × 3.10 mm, and the slice thickness was 44.299 μm. Since Dextran has an excitation maxima at 550 nm and emission maxima at 572 nm (Figure 11), the laser used was argon with excitation wavelengths at 496 nm and 514 nm, and its power was set to 20 % [48].

The analysis of the images acquired from confocal laser scanning microscopy was done with ImageJ, a program for image processing and analysis in Java. To determine the intensity profile when looking at the isotropic diffusion of Dextran from the solution in a well into the gel, the ”Radial profile plot extended” plugin was used. This plugin allows one to choose a starting line and an integration angle over which the integration on the defined ROI is done. This way, the radial intensity profile is obtained over the fan-shape area, instead of a line, which improves the statistics [50]. When viewing diffusion across a straight gel-gel interface, the intensity profile was obtained over a rectangular area. The intensity profile plots were created in Matlab. Each time series of intensity profile plots in this study is normalized to the maximum value of that individual series.

4 Results

4.1 Nanoparticle - hydrogel adhesion

In the specialization work, the adhesive properties of PDMA and agarose with various nanoparticles as glue were established: PDMA showed good gluing results for moderate amounts of MBA as chemical crosslinker, while agarose, on the other hand, could not be glued with nanoparticles. In this work we expanded the adhesion tests to alginate gels. The preparation of the alginate beads was successful, both with relatively small and large dimensions. However, the alginate beads could not be glued together with neither water, SM-50, or TM-50.

4.2 Interface permeability

4.2.1 Gel electrophoresis

The results from the electrophoresis experiments are presented in Figures 12 and 13. Figure 12a show separation of salmon sperm DNA (ssDNA) and ladder DNA on PDMA, imaged after 3 hours and 45 minutes. Figure 12b show the same experiment imaged after 6 hours. The gel was partially cut and glued with nanoparticles, creating a nanoparticle interface in lanes 1 to 5. The bands from the ssDNA have a reasonable intensity, while the DNA ladder has not. Notice how the migration of the ssDNA bands in lanes 3 to 5 is obstructed compared to lanes 8 to 10. Also, the intensity of the bands appear to have reduced with time. This could be due to photobleaching of the dye, or band broadening. Repeating this experiment showed that ssDNA was again hindered by the nanoparticle interface. However, along some sections of the interface the ssDNA actually did diffuse through.

In Figure 13a separation of ssDNA was done on agarose as a function of digestion time. Observe that the DNA digested for 5 minutes (lanes 3 and 4) traveled further than the undigested DNA (lanes 1 and 2). However, DNA samples digested for longer times are hardly visible in the gel. The run time was 54 minutes. Figure 13b also shows separation of ssDNA as a function of digestion time, but using shorter time intervals. One can observe that DNA digested for 2.5 and 5 minutes have traveled further than undigested DNA, in good argument with Figure 13a. The run time was 43 minutes. This experiment was repeated, now with electrophoretic separation on soft PDMA. In this case however, the undigested ssDNA was hardly visible, and the digested ssDNA not visible at all, independently of the digestion time (not shown). The run time was 3 hours.

4.2.2 Fluorescent molecule diffusion

The results from the introductory experiment probing the diffusion of food colorant are presented in Figure 14. The surface of the well is much sharper, and the color remains more intense inside the well, when there are nanoparticles present. There is also a sharper drop in intensity in an outward radial direction, compared to the

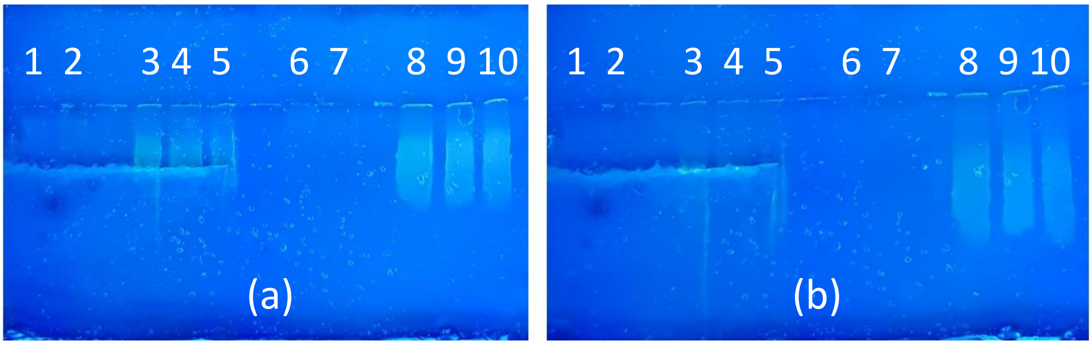

Figure 12: Electrophoretic separation of salmon sperm DNA (47 μg/mL) with average size $\leq$ 2,000 bp, and DNA ladder (62 μg/mL) with fragments ranging from 250 bp to 10,000 bp, on soft PDMA in TBE buffer. DNA samples were (lanes 1, 2, 6 and 7) DNA ladder, and (lanes 3-5 and 8-10) undigested Salmon Sperm DNA. Samples in lanes 1-5 were run through a layer of TM-50 particles. **a** Imaged after 3 hours and 45 minutes. **b** Same gel imaged after 6 hours.

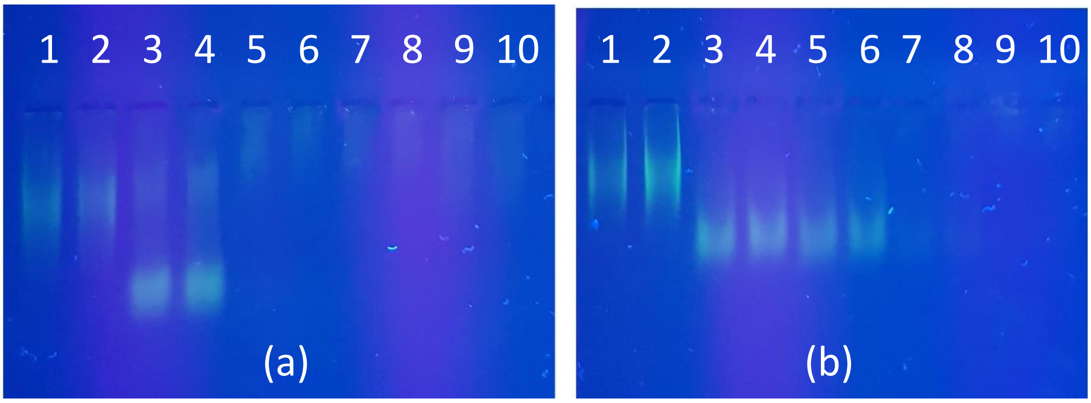

Figure 13: Electrophoretic separation of salmon sperm DNA (47 μg/mL) with average size $\leq$ 2,000 bp, as function of digestion. Separation on agarose in TBE buffer. **a** DNA samples were (lanes 1 and 2) undigested, (lanes 3 and 4) digested 5 minutes, (lanes 5 and 6) digested 10 minutes, (lanes 7 and 8) digested 15 minutes, and (lanes 9 and 10) digested 30 minutes. The run time was 54 minutes. **b** DNA samples were (lanes 1 and 2) undigested, (lanes 3 and 4) digested 2.5 minutes, (lanes 5 and 6) digested 5 minutes, (lanes 7 and 8) digested 7.5 minutes, and (lanes 9 and 10) digested 10 minutes. The run time was 43 minutes.

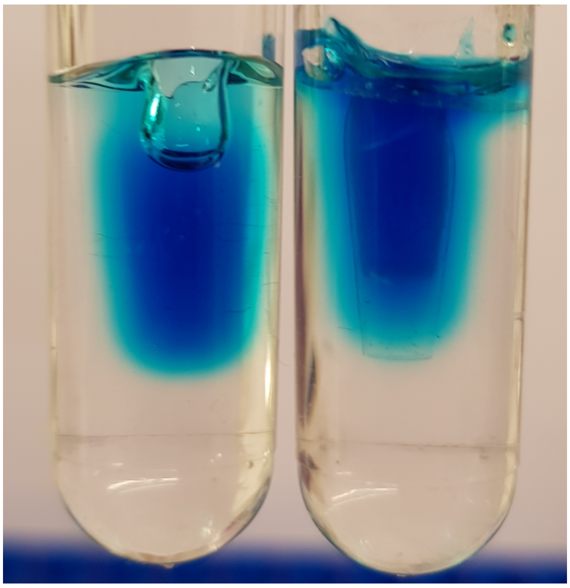

Figure 14: Diffusion of food colorant in PDMA gel. The well in the right tube was coated with nanoparticles (TM-50), while the well in the left tube was left bare. The picture was taken 55 minutes succeeding the application of food colorant in the wells.

gel with the bare well surface, where the density of food colorant looks more evenly distributed in the radial direction.

Because these results looked promising we have used fluorescent Dextran molecules and the setup described in Section 3.2.2 and depicted in Figure 10.

Solution-gel interface

Producing good results proved quite challenging with the initial setup (Figure 10a). In order to improve the experimental outcome, alterations have been done along the way, some of which are described in Figures 10b and 10c. The initial setup illustrated in Figure 10a did not work because the gel absorbed the solution from the wells, which caused the wells to dry out during image acquisition, which took up to 50 minutes.

This problem was approached by carving out a big portion of the gel, creating a reservoir for a relatively large amount of Dextran solution, as illustrated in Figure 10b. The PDMA gel was also consistently prepared as a hard gel, thus reducing gel swelling [16, 17, 19]. The results from this setup are presented in Figure 15. Figures 15a and 15c show the fluorescence intensity of Dextran over time, as it diffuses into PDMA gel, respectively in the presence or absence of a nanoparticle layer. The concentration of the Dextran solution was 0.195 mg/mL. The CLSM images in Figures 15b and 15d correspond to one intensity profile in Figures 15a and 15c, respectively. The initial conditions for the system were presumably similar to that illustrated in Figure 6. However, already after 5 minutes, the intensity was much higher in the gel than in the solution in the well, and increasing with time. Diffusion should only occur in a high-concentration to low-concentration fashion,

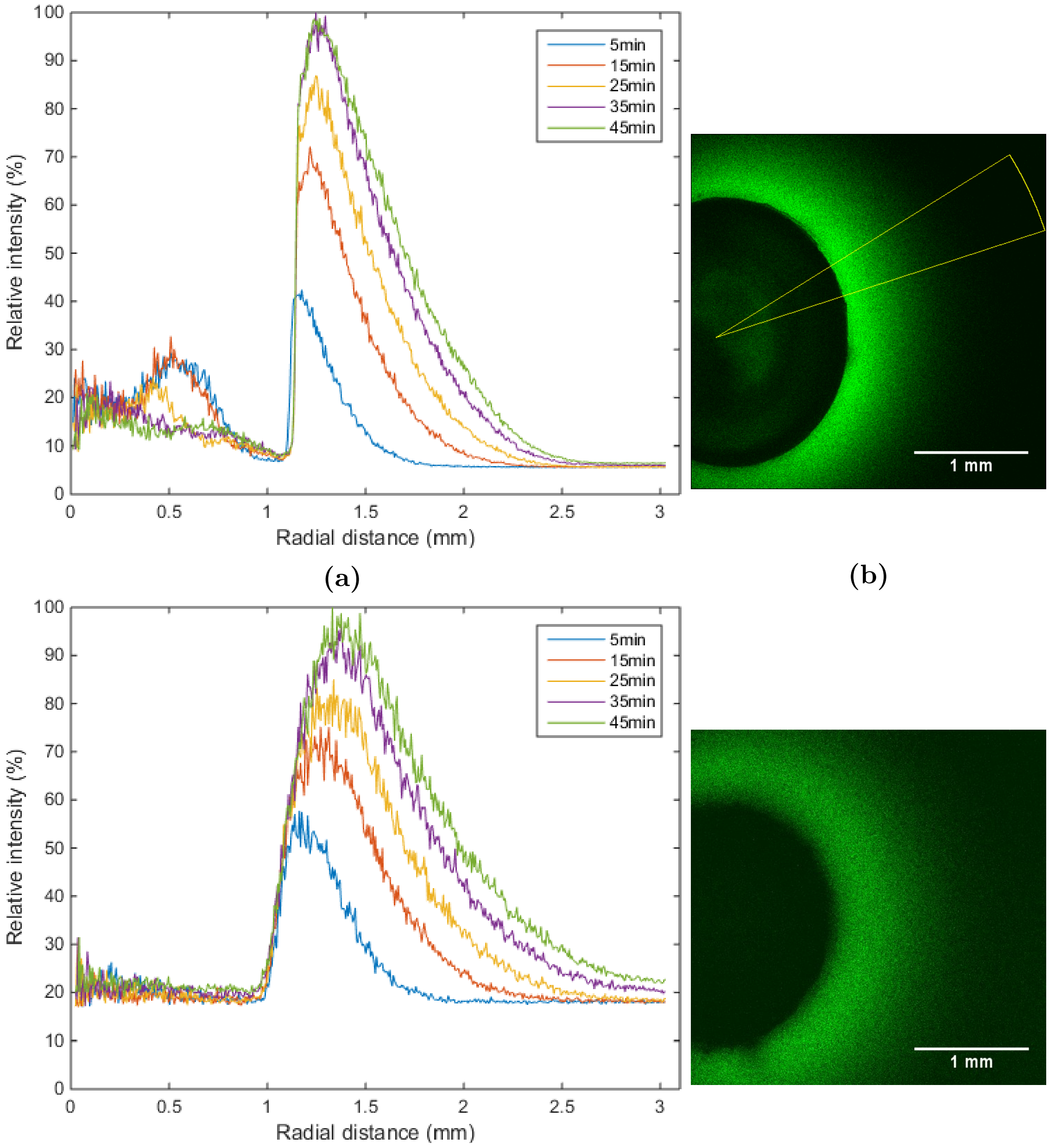

(a) (b)

(c) (d)

Figure 15: Intensity profile plots (left), with the corresponding CLSM images (right), of the solution-gel interface, showing intensity as a function of radial distance from the center of the well. The gel was hard PDMA, and the setup is described in Figure 10b. The confocal images (**b** and **d**) were taken after 25 minutes. **a** Nanoparticles (TM-50) are present at the surface of the well. **b** CLSM image corresponding to the yellow intensity curve in **a**. The yellow line marks the fan-shaped area of integration to generate the intensity profile. **c** No nanoparticles are present at the gel surface. **d** CLSM image corresponding to the yellow curve in **c**.

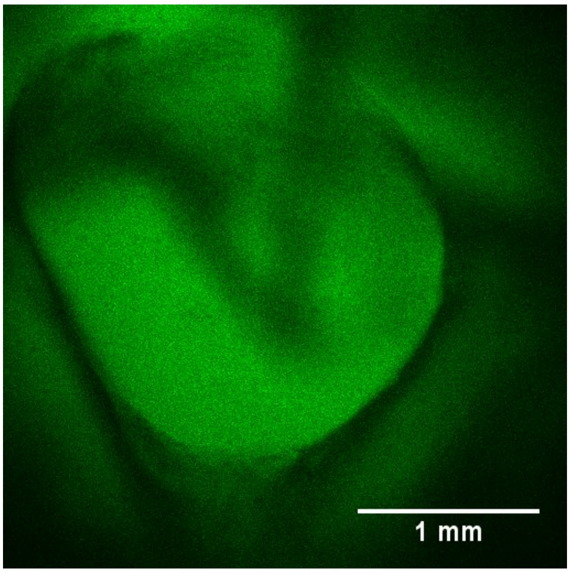

Figure 16: CLSM image of a solution-gel interface after 25 minutes. The gel was hard PDMA pre-swollen 17 hours, and the concentration of the Dextran solution was (0.39 mg/mL). There are no nanoparticles present at the surface of the well.

which means that here the gel swelling was quite severe, drawing Dextran into the gel regardless of the concentration gradient.

In order to separate the contributions from diffusion due to the gradient in Dextran and due to the swelling of the gel, the gel was pre-swollen. This was achieved by taking out the gel from the chamber slide and lowering it in water with the lid still on, in order to prevent the wells from closing up as a result of the swelling. The gel was equilibrated with water for 17 hours prior to the image acquisition. Figure 16 shows the CLSM image of a hard gel 25 minutes after addition of Dextran solution (0.39 mg/mL). As observed in the image, the swelling process left the well distorted, and the intensity profile would vary depending on how the area of integration was chosen. The intensity profile (not shown) did however look better than without pre-swelling, since the contribution of the gel swelling was reduced quite a bit. The plan was now to design a setup that both produces reproducible data, while incorporating pre-swelling of the gels.

Gel-gel interface

Using the setup described in Figure 10c, which involved equilibrating one hydrogel in Dextran solution and another in water, provided an interface with the same osmotic pressure on each side, thus taking swelling mechanisms out of the equation. In addition, the gel-gel interface was a better model for skin bridging. The experiment was also reproducible.

The hydrogels (hard PDMA) were prepared by placing one of them in Dextran solution and the other one in water, allowing them to swell for two days. The gels were cut into pieces with sizes ranging from 0.5 cm^3 to 1 cm^3, and pressed together at time 0. Figures 17b and 17d show a CLSM image of the diffusion of

Dextran molecules toward the gel equilibrated in water, and across an interface with and without nanoparticles, respectively. Figures 17a and 17c show the evolution of the corresponding intensity profile. The concentration of the Dextran solution was 0.0177 mg/mL, and the gel surfaces at the interface were rough, as illustrated in Figure 18.

One can observe from Figure 17 that at time close to 0 the fluorescence intensity is relatively high up to distances of about 1.2 mm, corresponding to the gel equilibrated with the Dextran solution, after which it decreases to a plateau with low intensity, where the gel was equilibrated with water. This profile is consistent with what would be expected from this type of systems (Figure 6). This difference in fluorescence intensity decreases with time, as the Dextran molecules diffuse towards the initially Dextran-free gel. As this happens, a drop in intensity occurs at the gel-gel interface, breaking up the neat diffusion curves. This intensity-drop appears to be wider and more significant in the presence (Figure 17a) than in the absence (Figure 17c) of nanoparticles. Another observation is that the intensity profile from the image captured after 12.5 minutes in Figure 17a (red line), does not follow the trend set by the other points in time, showing a higher intensity than expected.

An air-bubble was accidentally trapped in the interface in Figure 17d. The presence of the bubble indicates that the intensity-drop observed in the middle of the plots actually represents the interface between the hydrogels, as the bubble can be observed at the top of the CLSM image as a broadening of the dark vertical line. On a side note, in the case of the presence of the air-bubble, the area of interest for assessing the fluorescence intensity across the interface was chosen below the bubble to avoid this effect. Anyway, the relatively broad intensity-minima along the interface could be caused by some defects of the rough gel structure at the surface, since the piece of gel was cut from a larger hydrogel (Figure 18). The intensity-drop also appears to be broader in the presence, than in the absence of nanoparticles. Aiming to reduce the intensity-drop at the interface, the experiment was therefore repeated using gel pieces with clean surfaces, *i.e.*, surfaces that were facing the chamber slide during polymerization (Figure 18).

The results from the experiment, now with clean gel surfaces and Dextran solution concentration of 0.0093 mg/mL, are presented in Figure 19. In general, the intensity profiles of the gel-gel experiments are similar. The initial difference in intensity between the Dextran-equilibrated gel and the water-equilibrated gel is decreasing over time as expected, with the difference being larger for the systems with higher concentration of Dextran. The clean surfaces did not seem to have any effect on the intensity at the interface, as the intensity-drop again is observed, here around 1.5 mm in Figures 19a and 19c.

As mentioned, GelStar is a fluorescent dye that in the specialization work was found to interact with silica nanoparticles. We have thus used this property to assess the position of the nanoparticles in the gel-gel fluorescence interface. As the emission of GelStar is close to that of Dextran it was not possible to follow both dyes simultaneously. Figure 20 shows the intensity profile of the gel-gel interface glued by TM-50 nanoparticles pre-mixed with GelStar. Also here clean gel surfaces were used. Panel (a) refers to two gels that were glued directly, and panel (b)

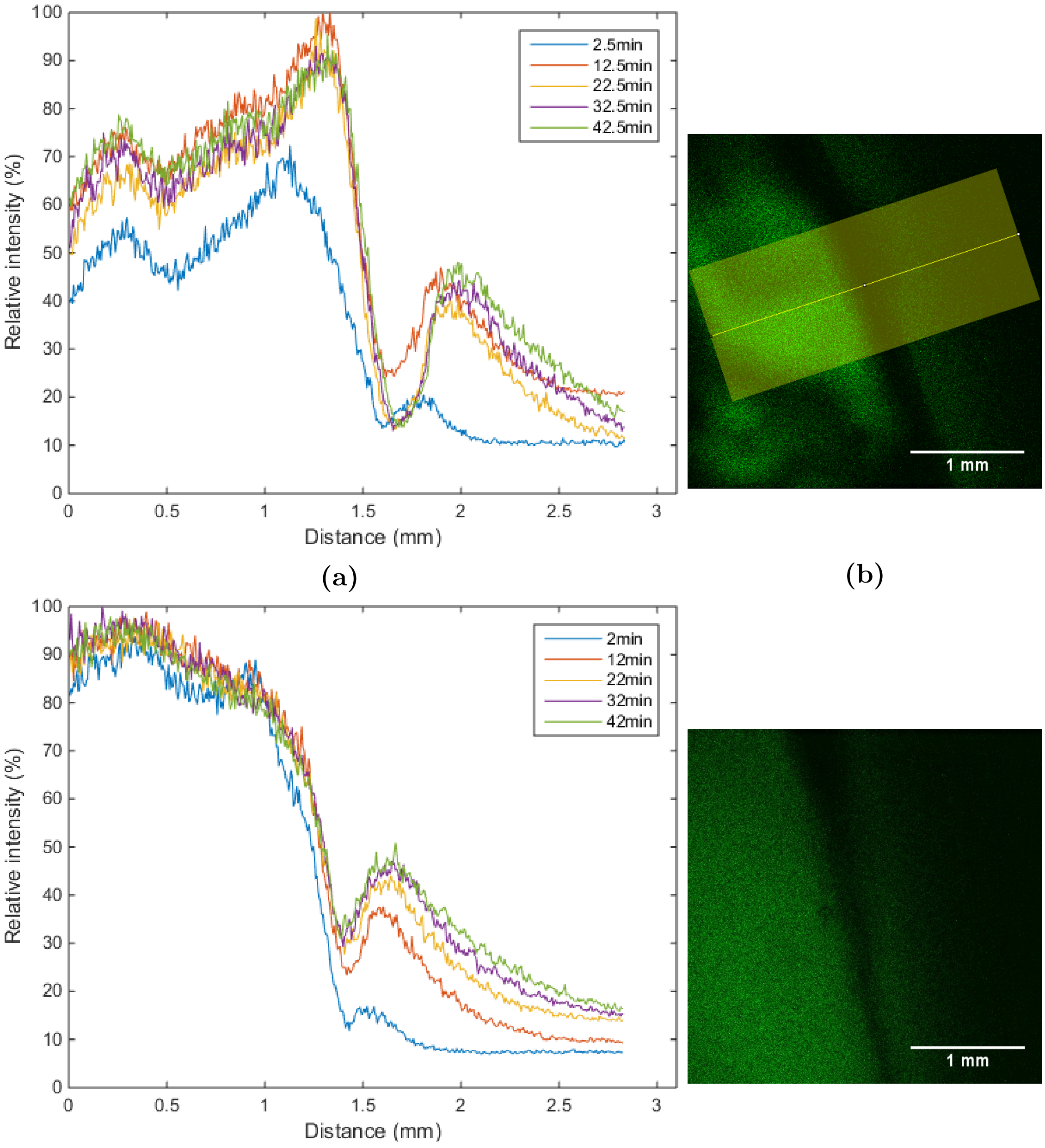

(a) (b)

(c) (d)

Figure 17: Intensity profile plots (left), with the corresponding CLSM images (right), of the gel-gel interface (Figure 10c), showing intensity as a function of distance. The gels were hard PDMA, one of which were equilibrated in Dextran solution (0.0177 mg/mL), and the other in water. The gel surfaces facing each other are rough surfaces. **a** Nanoparticles (TM-50) are present at the interface. **b** CLSM image taken 22.5 minutes after the gel pieces were pressed together, *i.e.*, corresponding to the yellow intensity curve in **a**. The yellow rectangle marks the area of integration for generating the intensity profiles. **c** No nanoparticles are present at the interface. **d** CLSM image taken after 22 minutes, corresponding to the yellow curve in **c**.

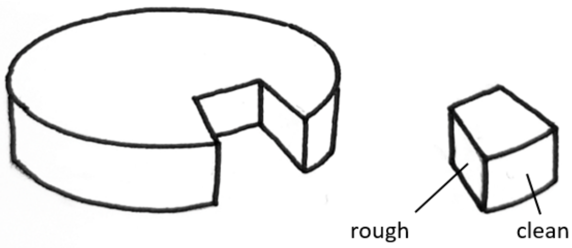

Figure 18: Illustration of the hydrogel pieces used in the gel-gel interface experiments. The "rough" surface has been cut with a scalpel, while the "clean" surface was facing the wall of the chamber slide during polymerization.

refers to gels that were glued after equilibration with water for 19 hours. The first observation is that there is a defined peak at the interface, so most nanoparticles do indeed accumulate there. The broadening of the intensity-peak in the case of the unswollen gels is assumably due to swelling forces drawing Dextran into the gel network (Figure 20a). These forces are considerably reduced in the case of the swollen gels, and a consequential narrower peak is observed (Figure 20b). Furthermore, it is also clearly visible in these plots that there is an increase in the background intensity with time.

In Figure 21 one can see the emission spectra for Dextran, Dextran in the presence of nanoparticles, and nanoparticles alone, excited at wavelengths corresponding to that of the laser used to illuminate the sample in the Leica SP5 microscope, namely $\lambda_{\text{ex}} = 496$ nm and $\lambda_{\text{ex}} = 514$ nm. One can observe that in the presence of nanoparticles (red and yellow line), there is an increase in the intensity of emission from Dextran, when compared to Dextran alone (blue and green). The emission is very low for the nanoparticles alone.

On a side note, it was experienced in previous work that exposure to oxygen would affect the proper polymerization of the PDMA, and the gel would become sticky and difficult to handle [16, 21, 22]. As an alternative to working in a nitrogen environment, custom-made lids were supplied and applied, as mentioned. This setup seem to have worked, as the gels handled quite well throughout the work.

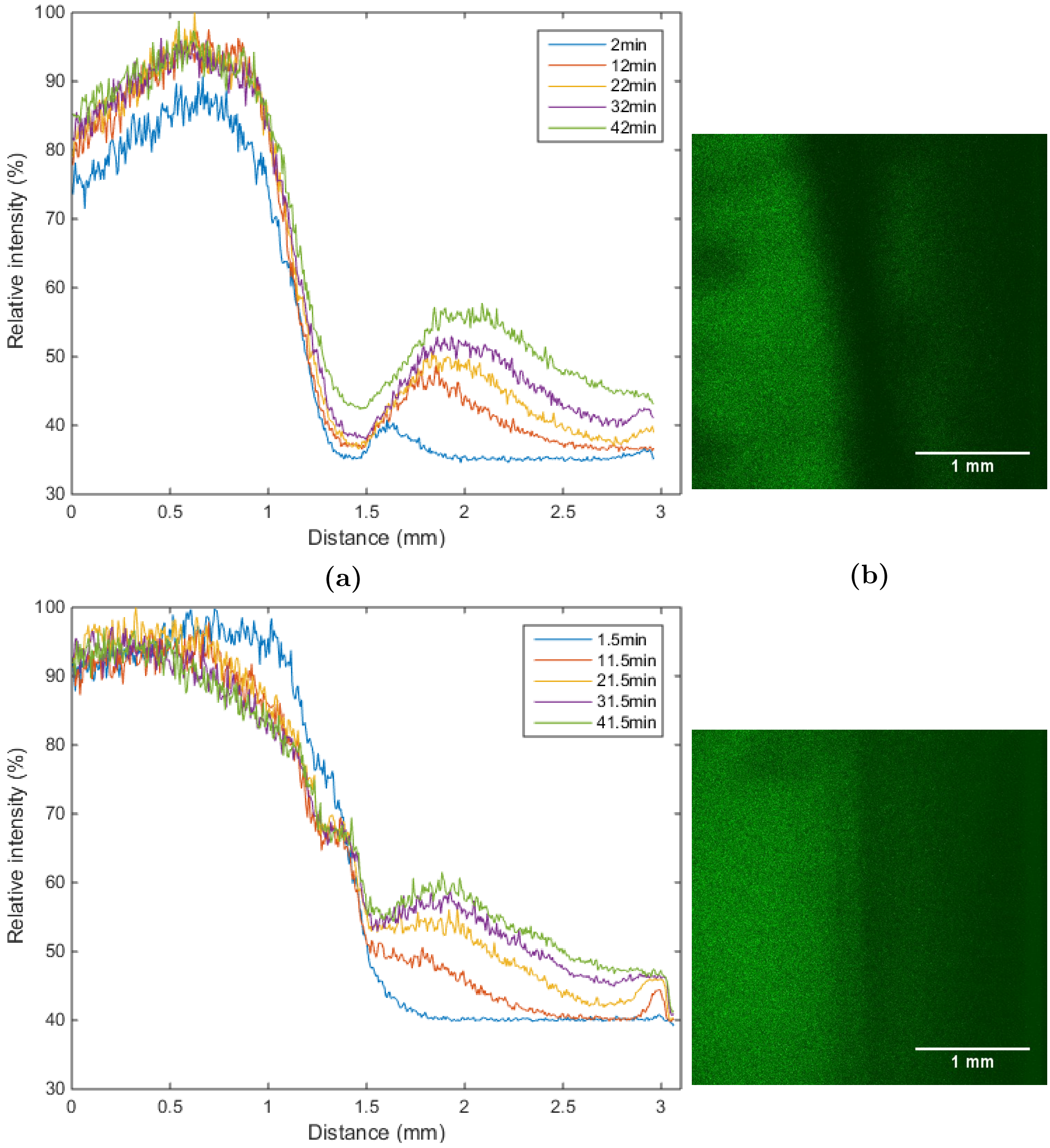

(a) (b)

(c) (d)

Figure 19: Intensity profile plots (left), with the corresponding CLSM images (right), of the gel-gel interface. This is a repetition of the experiment presented in Figure 17, but the concentration of the Dextran solution is now 0.0093 mg/mL, and the gel surfaces facing each other are clean surfaces. **a** Nanoparticles (TM-50) are present at the interface. **b** CLSM image taken 22 minutes after the gel pieces were pressed together, *i.e.*, corresponding to the yellow intensity curve in **a**. **c** No nanoparticles are present at the interface. **d** CLSM image taken after 21.5 minutes, corresponding to the yellow curve in **c**.

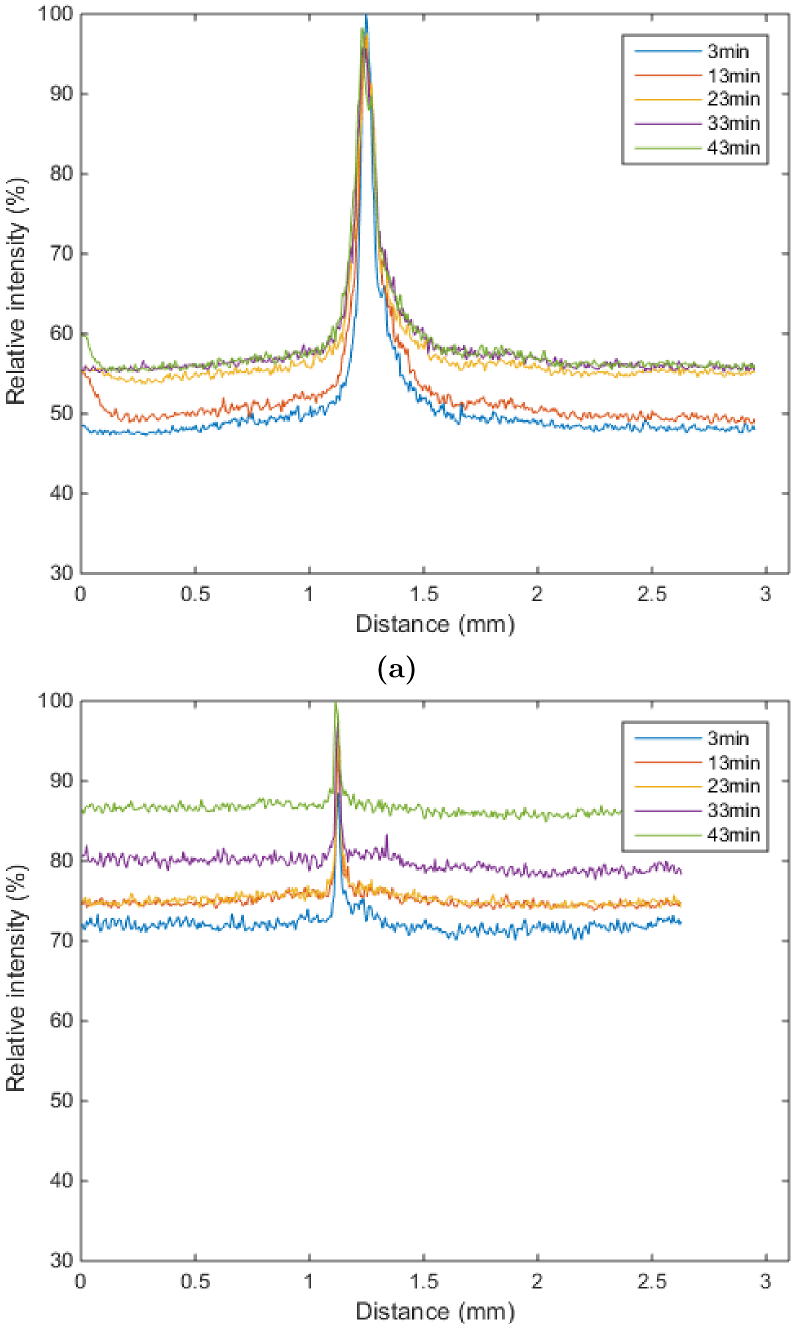

(a)

(b)

Figure 20: Intensity profile plots of the gel-gel interface. The gels were glued together with nanoparticles pre-mixed with GelStar. **a** Unswollen gels. **b** Gels swollen in water for 19 hours preceding the experiment.

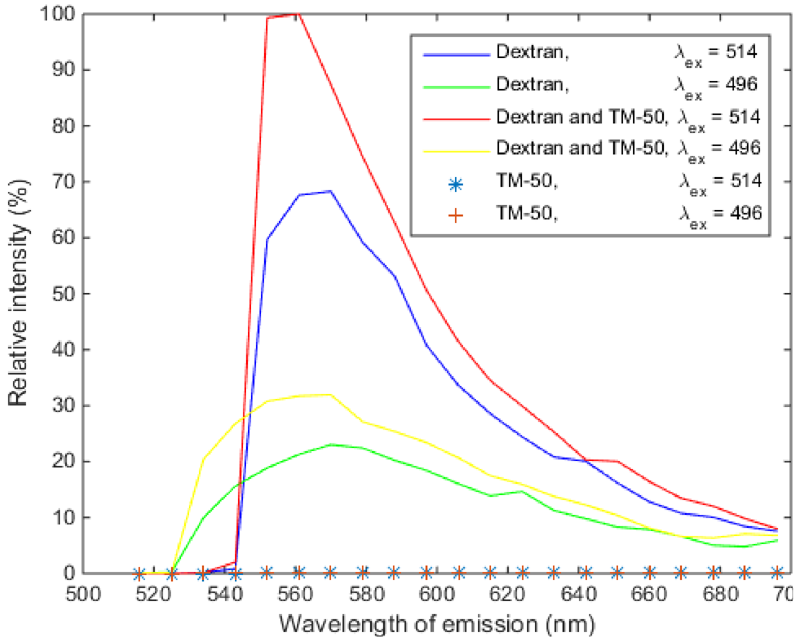

Figure 21: Emission spectra for Dextran, Dextran mixed with nanoparticles (TM-50), and for nanoparticles alone, when excited at either 496 nm or 514 nm, corresponding to the excitational wavelengths (λ_{ex}) of the argon laser used in the Leica SP5.

5 Discussion

5.1 Nanoparticle - hydrogel adhesion

Since PDMA, with moderate amounts of chemical crosslinker, has shown excellent absorption properties to TM-50 and SM-30 nanoparticles, it was considered the base for most of the conducted experiments.

An attempt was made to glue calcium alginate hydrogel beads with nanoparticles. It proved rather difficult to see whether or not the small alginate beads could be glued together with nanoparticles as they were too small to handle well. Therefore larger, teaspoon-sized particles were made. Unfortunately, we were not able to glue alginate beads together. This could be due to a number of reasons. The alginate may not possess the required chemical specificity to the silica surface and so the nanoparticles do not adsorb to it. It may also happen that the nanoparticles adsorb to the alginate network but the pores are too large and the particles diffuse from the surface (Figure 4c).

5.2 Interface permeability

The aim of this study was to determine the effect of the presence of nanoparticles on the diffusion of biomolecules, since Meddahi-Pellé *et al.* showed that the application method of nanoparticles could affect the healing process of a wound [7].

5.2.1 Gel electrophoresis

Figure 12 shows that the presence of nanoparticles in the interface does hinder the diffusion of large macromolecules. In the repeated experiment, the diffusion of ssDNA was obstructed, but only along portions of the interface. This may indicate that the amount of applied nanoparticles may have varied along the interface. It could also be due to the experienced difficulties concerning cutting and gluing the gel, since the PDMA tended to stick to the bottom of the casting tray. As migration is faster in buffer than in a hydrogel, gaps along the interface caused by poor wound edge approximation (the bringing-together of the gel wound edges), could increase migration velocity, or potentially cause the DNA molecules to travel out of the gel network and disappear in the buffer.

Previous work has shown that PDMA has a small mesh-size, so in order to reduce the electrophoresis run time, a soft gel was prepared, maximizing the pore-size. Nevertheless, the run time was quite long: 6 hours for the electrophoretic separation depicted in Figure 12. Therefore, electrophoretic separation of ssDNA on agarose, as a function of digestion time, was carried out. The results were quite promising (Figure 13). The degradation of the DNA fragments worked, and the now shorter fragments did travel faster in the agarose gel, than the undegraded DNA fragments. DNA incubated with DNase for times longer than 5 minutes could hardly be visualized. It may be that the interaction between DNA and GelStar is reduced by the altering of the chemistry of the DNA double helix from the hydrolytic cleavage catalyzed by DNase. Very small DNA fragments will therefore, although they travel faster in the hydrogel, be harder to visualize, as they bind to a smaller amount of fluorescent GelStar.

Having established the optimal digestion time of ssDNA with DNase to increase the velocity during electrophoresis, separation on PDMA was attempted (not shown). The undigested ssDNA did travel into the gel, but the digested ssDNA could not be visualized. Either it traveled too fast and left the hydrogel, or it had not bound to enough GelStar, possibly in combination with too long digestion time. Since the undigested ssDNA did travel in PDMA, although slowly, the digested DNA fragments were not pursued further.

5.2.2 Fluorescent molecule diffusion

The preliminary experiment performed with food colorant (Figure 14) indicated that the presence of nanoparticles may affect the rate of diffusion. This was therefore expanded by looking at the diffusion of a fluorescent biomolecule. In these experiments one would expect to observe an intensity profile similar to that depicted in Figure 6, with perhaps somewhat faster diffusion through the interface in the absence, than in the presence of nanoparticles.

Solution-gel interface

Studying the diffusion of relatively small fluorescent molecules across a liquid-gel interface covered with nanoparticles was very challenging. All in all, these experiments were not very successful.

Gel-gel interface

The experiments with diffusion through a gel-gel interface turned out to be a better method for studying diffusion of biomolecules through a nanoparticle interface, and also a better model for closure of skin wounds. One reason for the successful setup was that the medium was the same on both sides of the interface, with equal osmotic pressure, as the gels were swollen for the same amount of time. Thus, removing the contribution of the gel swelling to the diffusion. The setup is also reproducible, as can be seen by comparing Figures 17 and 19.

As mentioned in the results, the intensity profiles in Figures 17a, 17c, 19a and 19c show many similarities with the expected diffusion curve in Figure 6. One major difference is the intensity-minima. This could be due to defects in the gel-structure in the transition from one homogeneous gel to the other. This effect was observed both when using cut, rough gel surfaces (Figure 17), and when using clean gel surfaces (Figure 19).

The intensity-minima are more severe in the presence (Figures 17a and 19a), than in the absence (Figures 17c and 19c) of nanoparticles. This could be explained in view of the jump model. The nanoparticles are occupying the interface, resulting in an accumulation of fluorescent Dextran molecules right before the interface, and immediately after it, as they diffuse across it.

Another difference from the expected diffusion curve is the intensity-peak in the Dextran-rich gel in the presence of nanoparticles (Figures 17a and 19a), around 1.3 mm and 0.8 mm, respectively. One explanation for this accumulation of Dextran near the interface may be that Dextran interacts with nanoparticles. This theory is supported by the obtained emission spectra in Figure 21, where nanoparticles appear to interact with Dextran molecules, increasing the intensity of their emission. The presence of nanoparticles may accordingly increase the fluorescence intensity of Dextran molecules close to the interface in Figures 17a and 19a, giving rise to the intensity-peak. Additionally, the Dextran molecules' affinity toward nanoparticles may cause more Dextran to accumulate in the close proximity of the interface, thus increasing the intensity-peak further.

There is a moderate decrease of intensity with time in the Dextran-equilibrated gel in Figure 19c, which is in accordance with Figure 6. One would however expect a more than moderate decrease in the Dextran-equilibrated gel in all the plots (Figures 17 and 19). The explanation can be found in one general observation that the intensity seem to increase with time in all plots. It is particularly clear in Figure 20, where one can observe the background intensity in the water-equilibrated gels increase over time. It would make more sense to observe the opposite phenomenon, that the intensity of Dextran decreased with time due to photobleaching. Nevertheless, there are two possible explanations for why the intensity increases with time: (i) drifting of the laser output, or (ii) shrinking of the gel sample due to exposure to air, thus increasing the concentration of Dextran molecules in the image slice. It takes time for the argon laser output to stabilize after it has been switched on. The Leica SP5 with the 514 nm laser line has been shown to rapidly reach maximum laser output, and then slowly decrease and stabilize in about 3 hours [51]. Decreasing laser output with time would have the opposite effect on the intensity-profiles than what is observed in the plots. Theory (ii) is therefore a better explanation for the observed increase of intensity with time, as the hydrogels were equilibrated in solution for two days before placed in the chamber slide fully exposed, for up to 50 minutes of image acquisition.

All things considered, the shape of the intensity curves can still be used for comparison. Comparing Figure 17a with 17c, and Figure 19a with 19c, one can conclude that diffusion of relatively small biomolecules through the nanoparticle interface do occur. The nanoparticles do not seem to severely hinder the diffusion, which is promising for the application of nanoparticles in wound closure.

This methodology worked, but some improvements for further work can be suggested. To maintain a constant intensity with time, the chamber slides should have been filled up with water covering the gel samples during image acquisition, thus maintaining swelling-equilibrium. Curve fitting of the intensity profiles could also be explored, in order to develop a method for performing more of a quantitative analysis study, as it was not time for it in this work. The times at which the gel samples were imaged varies slightly, as the objective at all times was to initiate the time series acquisition as soon as possible, aiming to capture the initially sharp boundary (Figure 6). The setup should therefore be improved to allow for image acquisition from time zero. One way to improve the gel-gel experiment could be using a fluorescent molecule that does not interact with nanoparticles, and possibly a molecule within other size-ranges than what was seen here. It would also be very interesting to see a setup that reduces the observed intensity minima at the transition.

6 Conclusion

A large part of the work was dedicated to the optimization of the setup for assessing diffusion across gel interfaces covered with or glued by nanoparticles. With the gel electrophoresis setup it could be concluded that the methodology followed, by gluing gels with a nanoparticle aqueous suspension, somewhat hindered the transport of large ($\leq$ 1,320 kg/mol) DNA molecules.

Gluing two pre-swollen gels with nanoparticle suspension was found to be the best setup to study the transport of fluorescent Dextran molecules with relative low molecular weight (4.4 kg/mol) down its concentration gradient. This was the method that gave more reproducible results and the one that best models wound-closing *in vivo*. It was found that the nanoparticles applied as a suspension remain in the (broad) interface and do not significantly affect the diffusion of Dextran across it.

Bibliography

1. Jayesh, B. S. The History of Wound Care. *Journal of the American College of Certified Specialists,* 65–66 (2011).
2. Tritle, N. M., Haller, J. R. & Gray, S. D. Aesthetic Comparison of Wound Closure Techniques in a Porcine Model. *The Laryngoscope,* 1949–1951 (2001).
3. Custis, T., Armstrong, A. W., King, T. H., Sharon, V. R. & Eisen, D. B. Effect of Adhesive Strips and Dermal Sutures vs Dermal Sutures Only on Wound Closure. *JAMA Dermatol,* 862–867 (2015).
4. Zhang, W., Xue, D., Yin, H., Xie, H., Ma, H., Chen, E., Hu, D. & Pan, Z. Barbed versus traditional sutures for wound closure in knee arthroplasty: a systematic review and meta-analysis. *Scientific Reports* (2016).
5. Dumville, J. C., Coulthard, P., Worthington, H. V., Riley, P., Patel, N., Darcey, J., Esposito, M., van der Elst, M. & van Waes, O. J. Tissue adhesives for closure of surgical incisions. *Cochrane Database of Systematic Reviews* (2014).
6. Sundby, C. N. Wound Closure (2017).
7. Meddahi-Pellé, A., Legrand, A., Marcellan, A., Louedec, L., Letourneur, D. & Leibler, L. Organ Repair, Hemostasis, and In Vivo Bonding of Medical Devices by Aqueous Solutions of Nanoparticles (2014).
8. Stöber, W., Fink, A. & Bohn, E. Controlled Growth of Monodisperse Silica Spheres in the Micron Size Range. *Journal of Colloid and Interface Science,* 62–69 (1968).
9. Danks, R. R. *Wound Closure Technique* `http://emedicine.medscape.com/article/1836438-overview`. [Online: 2017-09-28].
10. Dobson, P., King, S. & Jarvie, H. *Nanoparticle* `https://www.britannica.com/science/nanoparticle`. [Online: 2017-10-31].
11. Barisik, M., Atalay, S., Beskok, A. & Qian, S. Size Dependent Surface Charge Properties of Silica Nanoparticles. *The Journal of Physical Chemistry* **118,** 1836–1842 (2014).
12. Mamaeva, V., Sahlgren, C. & Linden, M. Mesoporous silica nanoparticles in medicine - Recent advances. *Advanced Drug Delivery Reviews,* 689–702 (2013).
13. Ahmed, E. M. Hydrogel: Preparation, characterization, and applications: A review. *Journal of Advanced Research,* 105–121 (2015).
14. Cruz-chu, E. R., Aksimentiev, A. & Schulten, K. *Amorphous silica* `http://www.ks.uiuc.edu/Research/silica/`. [Online: 2017-12-15].
15. Merck. *Colloidal Silica* `http://www.merck-performance-materials.com/en/electronic_materials/glossary/colloidal_silica/colloidal_silica.html`. [Online: 2017-12-05].
16. Carlsson, L., Rose, S., Hourdet, D. & Marcellan, A. Nano-hybrid self-crosslinked PDMA/silica hydrogels. *Soft Matter,* 3619–3631 (2010).
17. Næss, S. N., Mikkelsen, A., Elgsæter, A. & Dias, R. d. S. Molecular Biophysics. *Department of Physics, NTNU* (2016).
18. Cipriano, B. H., Banik, S. J., Sharma, R., Rumore, D., Hwang, W., Briber, R. M. & Raghavan, S. R. Superabsorbent Hydrogels That Are Robust and Highly Stretchable. *Macromolecules,* 4445–4452 (2014).
19. Brannon-Peppas, L. & Peppas, N. A. Equilibrium Swelling Behaviour of pH-sensitive Hydrogels. *Chemical Engineering Science* **46,** 715–722 (1991).
20. Sigma-Aldrich. *N,N'-Methylenebis(acrylamide)* `https://www.sigmaaldrich.com/catalog/product/sial/146072?lang=en&region=NO`. [Online: 2017-11-22].
21. Rose, S., Prevoteau, A., Elziére, P., Hourdet, D., Marcellan, A. & Leibler, L. Nanoparticle solutions as adhesives for gels and biological tissues. *Nature,* 382–385 (2013).

22. Sudre, G., Hourdet, D., Cousin, F., Creton, C. & Tran, Y. Structure of surfaces and interfaces of Poly(N,N-dimethylacrulamide) hydrogels. *Langmuir,* 12282–12287 (2012).

23. Sheehan, D. *Physical Biochemistry: Principles and Applications* ISBN: 9780470856024 (Wiley-Blackwell, 2009).

24. Arnott, S., Fulmer, A., Scott, W. E., Dea, I. C. M., Moorhouse, R. & Rees, D. A. The Agarose Double Helix and Its Function in Agarose Gel Structure. *Journal of Molecular Biology,* 269–284 (1974).

25. Viovy, J.-L. Electrophoresis of DNA and other polyelectrolytes: Physical mechanisms. *Reviews of Modern Physics,* 813–872 (2000).

26. Lee, B.-B., Ravindra, P. & Chan, E.-S. Size and Shape of Calcium Alginate Beads Produced by Extrusion Dripping. *Chemical Engineering and Technology* **36,** 1627–1642 (2013).

27. Rupérez, P., Ahrazem, O. & Leal, A. J. Potential Antioxidant Capacity of Sulfated Polysaccharides from Edible Marine Brown Seaweed *Fucus vesiculosus. Journal of Agricultural and Food Chemistry* **50,** 840–845 (2002).

28. Rinaudo, M. Biomaterials based on a natural polysaccharide: alginate. *TIP Revista Especializada en Ciencias Químico-Biológicas* **17,** 92–96 (2014).

29. Golmohamadi, M. & Wilkinson, K. J. Diffusion of ions in a calcium alginate hydrogel-structure is the primary factor controlling diffusion. *Carbohydrate Polymers* **94,** 82–87 (2013).

30. Netz, R. R. & Andelman, D. Neutral and Charged Polymers at Interfaces. *Physics Reports,* 1–95 (2003).

31. Cao, Z. & Dobrynin, A. V. Nanoparticles as Adhesives for Soft Polymeric Materials. *Macromolecules,* 3586–3592 (2016).

32. Tang, J., Li, J., Vlassak, J. J. & Suo, Z. Adhesion between highly stretchable materials. *Soft Matter,* 1093–1099 (2016).

33. Martin, P. Wound Healing - Aiming for Perfect Skin Regeneration. *Science* (1997).

34. Addgene. *Agarose Gel Electrophoresis* `https://www.addgene.org/protocols/gel-electrophoresis/`. [Online: 2017-10-30].

35. Brenner, S. & Miller, J. H. *Encyclopedia of Genetics* (2001).

36. Lonza. *Gelstar Nucleic Acid Gel Stain* `https://www.lonza.com/products-services/bio-research/electrophoresis-of-nucleic-acids-and-proteins/nucleic-acid-electrophoresis/nucleic-acid-gel-stains/gelstar-nucleic-acid-gel-stain-10000x.aspx`. [Online: 2018-03-01].

37. Philibert, J. One and a Half Century of Diffusion: Fick, Einstein, before and beyond. *Diffusion Fundamentals 2* **2,** 1–10 (2005).

38. Holde, K. E. v., Curtis, J. W. & Ho, P. S. *Principles of Physical Biochemistry* ISBN: 0-13-046427-9 (Pearson Education, Inc, 2006).

39. Gorban, A. N., Sargsyan, H. P. & Wahab, H. A. Quasichemical Models of Multicomponent Nonlinear Diffusion. *Mathematical Modelling of Natural Phenomena* **6,** 184–262 (2011).

40. Murphy, D. B. & Davidson, M. W. *Fundamentals of Light Microscopy and Electronic Imaging* (Wiley-Blackwell, 2012).

41. Bjørkøy, A. Instruction manual for Leica SP5 CLSM (2016).

42. Leica. *The Only Broadband Confocal Leica TCS SP5* `https://www.leica-microsystems.com/typo3temp/_processed_/c/d/csm_TCS_SP5_1_0928363c21.png`. [Online: 2018-03-02].

43. Jonkman, J., Brown, C. M. & Cole, R. W. Chapter 7 - Quantitative confocal microscopy: Beyond a pretty picture. *Methods in Cell Biology* **123,** 113–134 (2014).

44. Paddock, S. W. Confocal Laser Scanning Microscopy. *Biotechniques* **27,** 992–1004 (1999).

45. Zou, Y., Celli, A., Zhu, H., Elmahdy, A., Cao, Y., Hui, X. & Maibach, H. Confocal laser scanning microscopy to estimate nanoparticles' human skin penetration in vitro. *International Journal of Nanomedicine* **12,** 8035–8041 (2017).
46. Sigma-Aldrich. *Ludox TM-50 colloidal silica* `https://www.sigmaaldrich.com/catalog/product/aldrich/420778?lang=en&region=NO`. [Online: 2017-12-10].
47. Sigma-Aldrich. *Ludox SM colloidal silica* `https://www.sigmaaldrich.com/catalog/product/aldrich/420794?lang=en&region=NO`. [Online: 2017-12-10].
48. Sigma-Aldrich. *FITC-labelled polysaccharides* `https://www.sigmaaldrich.com/technical-documents/articles/chemistry/fluorescently-labeled-dextrane.html`. [Online: 2018-03-01].
49. Thermo-Fischer. *Fluorescence SpectraViewer* `https://www.thermofisher.com/no/en/home/life-science/cell-analysis/labeling-chemistry/fluorescence-spectraviewer.html?SID=srch-svtool&UID=2761old_2`. [Online: 2018-02-19].
50. Carl, P. *Radial Profile Extended* `https://imagej.nih.gov/ij/plugins/radial-profile-ext.html`. [Online: 2018-04-05].
51. Sporsheim, B. *Quantitative confocal laser scanning microscopy: optimization for in vivo and in vitro analysis of intracellular transport* (NTNU Grafisk senter, 2015).